A WIRELESS AND BATTERY-LESS SYSTEM FOR MONITORING CEREBROSPINAL FLUID SHUNTS

by

Anand Subramanian Narayanaswamy

APPROVED BY SUPERVISORY COMMITTEE

Dr. Mehrdad Nourani, Chair

Dr. Lakshman S. Tamil

Dr. Issa M.S. Panahi

Dr. Gil S. Lee

To my family

A WIRELESS AND BATTERY-LESS SYSTEM FOR MONITORING CEREBROSPINAL FLUID SHUNTS

by

ANAND SUBRAMANIAN NARAYANASWAMY

DISSERTATION

Presented to the Faculty of

The University of Texas at Dallas

in Partial Fulfillment

of the Requirements

for the Degree of

DOCTOR OF PHILOSOPHY IN

ELECTRICAL ENGINEERING

THE UNIVERSITY OF TEXAS AT DALLAS

December 2015

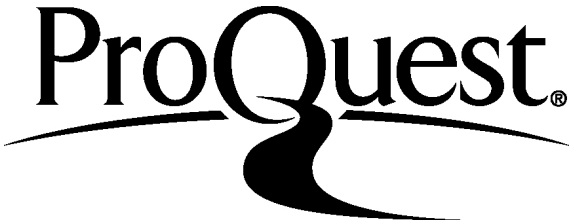

ACKNOWLEDGEMENTS

I am forever indebted to my advisor, Dr. Mehrdad Nourani for providing me the opportunity for working on this research. Without his great guidance, encouragement, feedback and patience this work could not be completed.

I am also grateful for Dr. Lakshman Tamil who is also a part of my committee for his valuable suggestions and technical advice on various topics in my research. His suggestions were very useful in completing my work and in my life. I would like to thank my committee members Dr. Issa M. S. Panahi and Dr. Gil Lee for their suggestion on improving my thesis.

I am very grateful to all members of the Quality of Life Technology lab at UTD for their friendship and help. Talking to labmates with different perspective helped me a lot in taking forward my research. I also want to thank Dr. Bill Swartz for his help and encouragement when I was his TA.

I would like to thank all my friends who helped to make my stay away from home very comfortable. Special mention for Aravind Rajendran who always had some suggestions when things are not working properly or talking something totally not related to take my mind off things for a while. Also I would like thank the new friends I made in Dallas especially Shejo Abraham for his help and encouraging words.

I would like to thank my family for the support they gave me to finish this work. My parents were very supportive and encouraging when I found going tough. My brother by his usual wits made me smile during my bad times. I would especially thank my aunt Rani Mahadevaiyer for her support and are and giving me a home away from home in Chicago when I am feeling home sick. I would also like to thank my other aunt Usha Narayan and my uncle Narayan for their suggestions and advice. Also my uncle Natarajan Mahadeva Iyer helped me a lot in technical details regarding my research and aunt Mini Natarajan for packing me at least a week's food when I am returning to Dallas from Albany.

Last but not the least, I am grateful to my wife, Vineetha Sivadasan for her unconditional love and care. Her support in the last few years helped me to finish my thesis. I would also like to thank her parents for their understanding and support.

July 2015

A WIRELESS AND BATTERY-LESS SYSTEM FOR MONITORING

CEREBROSPINAL FLUID SHUNTS

Publication No. _____

Anand Subramanian Narayanaswamy, Ph.D.
The University of Texas at Dallas, 2015

Supervising Professor: Mehrdad Nourani

This work presents a wireless and battery-less clog detection and flow measurement system for hydrocephalus shunts. Hydrocephalus is a condition where excess of cerebrospinal fluid (CSF) is accumulated in the brain. This is treated by diverting excess of CSF using an implanted shunt to another part of the body. The shunt catheter has an inside diameter of 1 mm and a thickness of 0.5 mm.

At present, the failure rate of shunts is more than 50% in the first two years after implant. This work presents a prototype system that will detect the location of clog in the shunt, thus increasing the reliability and diagnosability of the current system. The system also monitors the CSF flow rate through the shunt. This information can be used to adjust the programmable valve in the shunts to optimize the flow rate after shunt placement. Additionally, the system can measure other parameters like Intracranial Pressure (ICP), Intra-abdominal Pressure (IAP), and the pressure inside other locations in the shunt such as valve opening pressure. Monitoring the

above parameters will help to better understand the shunt hydrokinetics and design better shunts in future.

The proposed system uses multiple pressure sensors inside the shunt catheters for sensing the location of clog. The pressure differences between two sensors are used to calculate the flow of CSF in the shunt. With the data reported by the sensors, Bernoulli's equation and principle of fluid mechanics are used to reliably calculate the CSF flow rate. For better form factor and reliability, a system powered from outside of skin is proposed. The implanted sensor system harvests power from the RFID reader device placed outside the body and transmits the sensor data back to the RFID reader Our platform displays the location of clog and the rate of flow through a customized graphical user interface in a PC. Based on our experimental data, the accuracy of the clog detection is 100% for full occlusion. The flow measurement is 90% accurate when compared with the ground truth flow measured by a flow meter.

TABLE OF CONTENTS

LIST OF FIGURES

LIST OF TABLES

CHAPTER 1

INTRODUCTION

1.1 Hydrocephalus

Hydrocephalus is a medical condition which causes excessive accumulation of cerebrospinal fluid (CSF) in the brain. The excessive accumulation of CSF can cause abnormal widening of spaces (ventricles) in the brain. The widening of ventricles generates a potentially harmful pressure on the tissues of the brain [1], [2].

CSF is the fluid that surrounds the brain and spinal cord. CSF is a clear and colorless fluid which contains small quantities of glucose and protein. Ependyma, an epithelial membrane in the central nervous system (CNS) is involved in the production of CSF. The viscosity and density of CSF is very similar to water. CSF is a Newtonian fluid with viscosity range between 0.7 mPa.s - 1 mPa.s at 37º C [42]. The specific gravity of CSF in normal human being at 37º C is between 1.0063-1.0075 [43]. It is believed that about 500 ml of CSF is produced at the rate of 0.3 - 0.5 ml/min[3]. The amount of CSF present in brain at a given time is about 150 ml. The ventricular system in the brain consists of four ventricles interconnected by narrow passages. In normal condition CSF flows through the ventricles, exits into cisterns (closed spaces that serve as reservoirs) at the base of the brain. After that CSF bathes the surfaces of the brain and spinal cord, it is reabsorbed into the bloodstream. The main functions of CSF are to 1) act as a cushion or shock absorber and to keep the brain tissue buoyant, 2) deliver nutrients to brain and removing

waste, and 3) compensate for changes in intracranial blood volume by flowing between cranium and spine.

CSF is produced continuously in the brain; hence the balance between production and absorption of CSF is critical in maintaining the pressure inside the brain. Any medical conditions that block the normal flow or reabsorption of CSF will result in its over-accumulation. The resulting increased pressure of the fluid against brain tissue is the cause of hydrocephalus.

There are different types of hydrocephalus based on various classifications. One type of classification is congenital or acquired [4]. Congenital hydrocephalus is present in newborns and is caused by genetic abnormalities or due to some events in the fetal development. Hydrocephalus can be acquired at some point after birth. This type of hydrocephalus may be caused by injury or disease. Another classification is communicating or non-communicating. When CSF is blocked after it exits the ventricle, communicating hydrocephalus occurs. CSF can still flow between the ventricles, which remain open. When the flow of CSF is blocked along one or more of the narrow passages connecting the ventricles non-communicating hydrocephalus occur. It is also called "obstructive" hydrocephalus. One of the most common causes of hydrocephalus is from narrowing of the aqueduct of Sylvius, a small passage between the third and fourth ventricles in the middle of the brain. Another form of hydrocephalus is the Normal Pressure Hydrocephalus (NPH). NPH may result from a subarachnoid hemorrhage, head trauma, infection, tumor, or complications of surgery that cause an abnormal increase of cerebrospinal fluid in the brain's ventricles.

Symptoms of hydrocephalus depend on many factors. It varies depends on age, disease progression and individual tolerance to the condition. As the ability to compensate for increased pressure differs from infants to adults. Infant skull can expand to accommodate the buildup. Older children and adults, skulls cannot expand to accommodate buildup of CSF.

In infancy, the most obvious symptom of hydrocephalus is often an unusually large head size due to expansion of skull. Other symptoms [2] such vomiting, sleepiness, irritability, downward deviation of the eyes (sun setting), and seizures may be also present. In older children and adults symptoms such as headache followed by vomiting, nausea, blurred or double vision, sun setting of the eyes, problems with balance, poor coordination, gait disturbance, urinary incontinence, slowing or loss of developmental progress, lethargy, drowsiness, irritability, or other changes in personality or cognition including memory loss may be present. Symptoms of normal pressure hydrocephalus include problems with walking, impaired bladder control leading to urinary frequency and/or incontinence, and progressive mental impairment and dementia. An individual with this type of hydrocephalus may have a general slowing. Doctors may use a variety of tests, including brain scans such as computed tomography (CT) and magnetic resonance imaging (MRI), a spinal tap or lumbar catheter, intracranial pressure monitoring, and neuropsychological tests, to help them accurately diagnose normal pressure hydrocephalus and rule out any other conditions.

1.2 Diagnosis and Treatment

Hydrocephalus is diagnosed [2] using cranial imaging techniques such as ultrasonography, CT, MRI, or pressure-monitoring techniques. A physician selects the appropriate diagnostic tool based on an individual's age and condition.

Hydrocephalus is most often treated by surgically inserting a shunt system which diverts the excessive CSF from the brain to another part of the body like abdomen. A shunt is a flexible but sturdy tube made with bio-compatible material. A shunt system consists of a proximal catheter, a valve and a distal catheter. One end of the proximal catheter is placed within a ventricle inside the brain and the farther end of the distal catheter is commonly placed within the abdominal cavity where the CSF can drain and be absorbed. A valve connected between the proximal and the distal catheter maintains unidirectional CSF flow and regulates the CSF flow rate [62].

Figure 1.1 shows the surgical process for the shunt implant. A cut is made near the top of the head and another near the belly. A small hole is drilled in the skull and the proximal catheter (ventricular catheter) is placed into one of the ventricle. Distal catheter (peritoneal catheter) is placed under the skin behind the ear to the peritoneal cavity. A valve that attaches both the catheters is placed underneath the skin behind the ear. Figure 1.2 depicts the position of shunt after the surgery. The extra tubing is placed inside the abdomen in order to account for child growth.

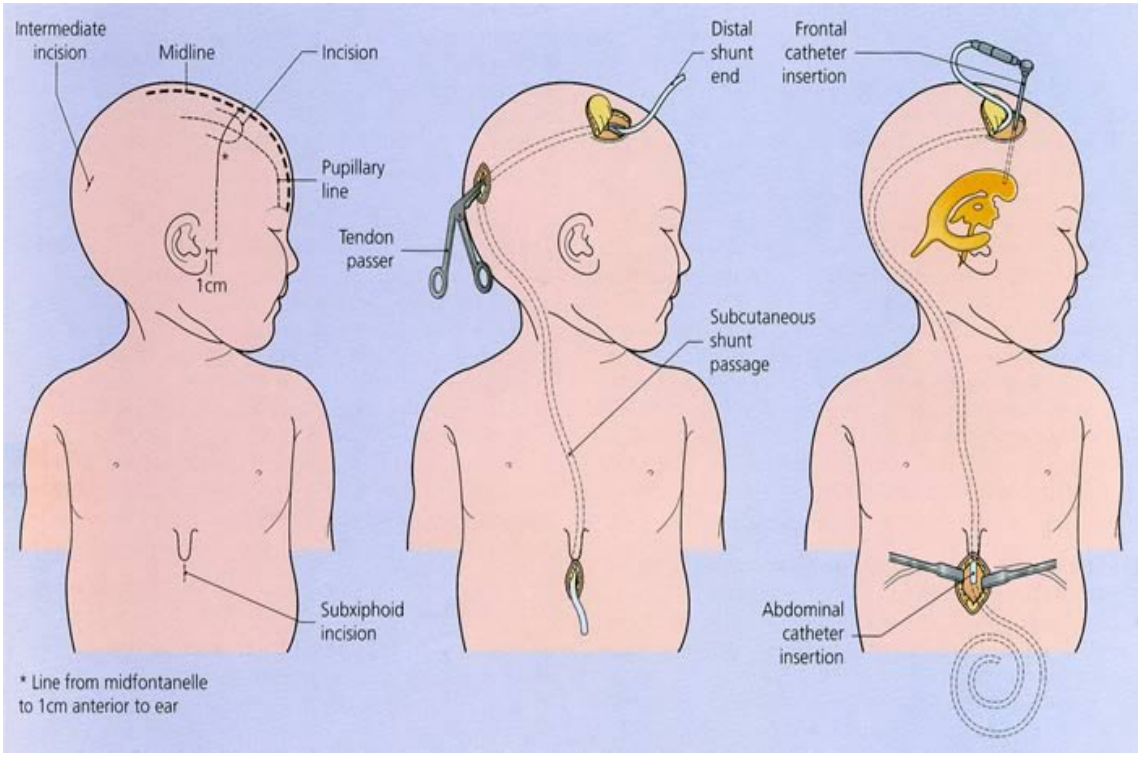

Figure 1.1. Surgical placement of shunt. (http://www.seattlechildrens.org/)

Figure 1.3 shows the shunt system components with a detailed diagram of the flow control valve [5]. Figure 1.3(a) shows the different components in the shunt. Figure 1.3 (b) shows the valve which allows CSF to drain from the brain to peritoneal cavity (one-way). Figure 1.3(c) shows the detailed picture of the variable pressure valve which can be controlled using magnetic tools.

Figure 1.4(a) shows a CT image of a brain with CSF build-up in the ventricles (dark area in the middle) before shunt placement. When a shunt is implanted in a person with hydrocephalus, CSF will be drained by the shunt, and the flow will be regulated so that a

constant intracranial pressure (ICP) is maintained within the brain. Figure 1.4(b) shows a post-operation CT image of the same patient's brain after shunt placement. The ventricles have drained and have resumed their normal size. The white area in the middle of the image is the catheter inside the ventricle.

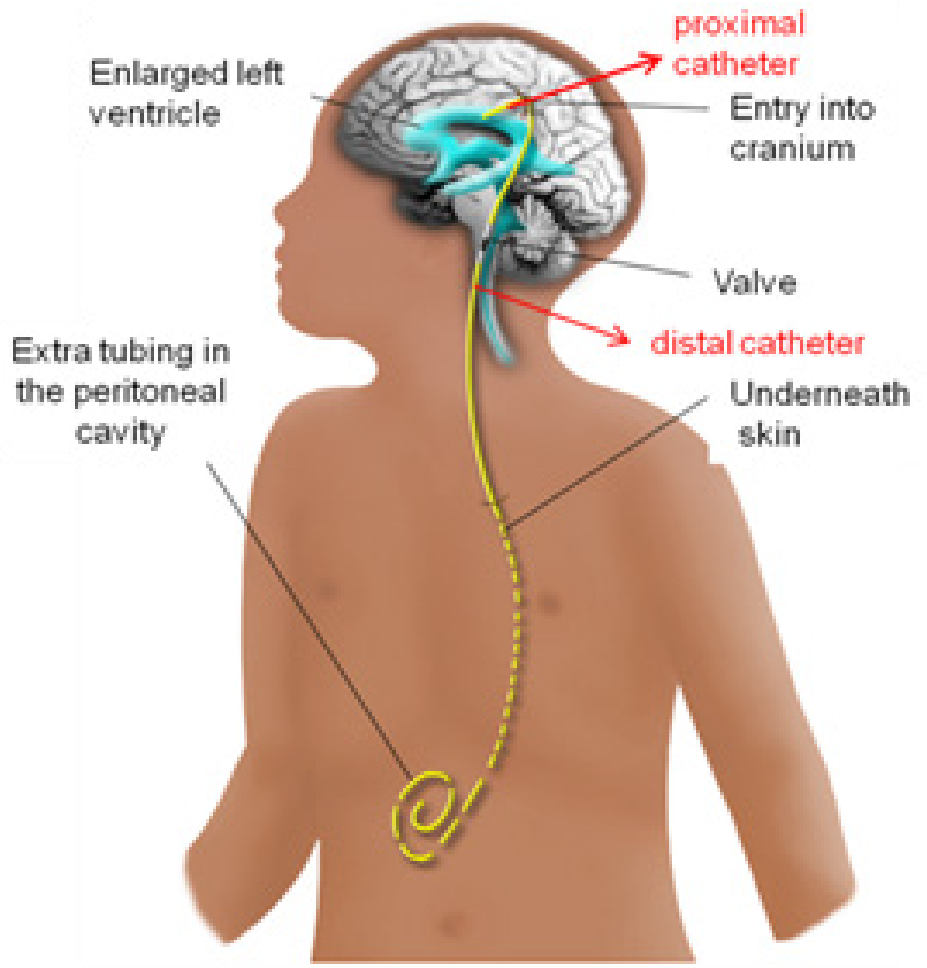

Figure 1.2. The shunt catheter after the surgery (from [37])

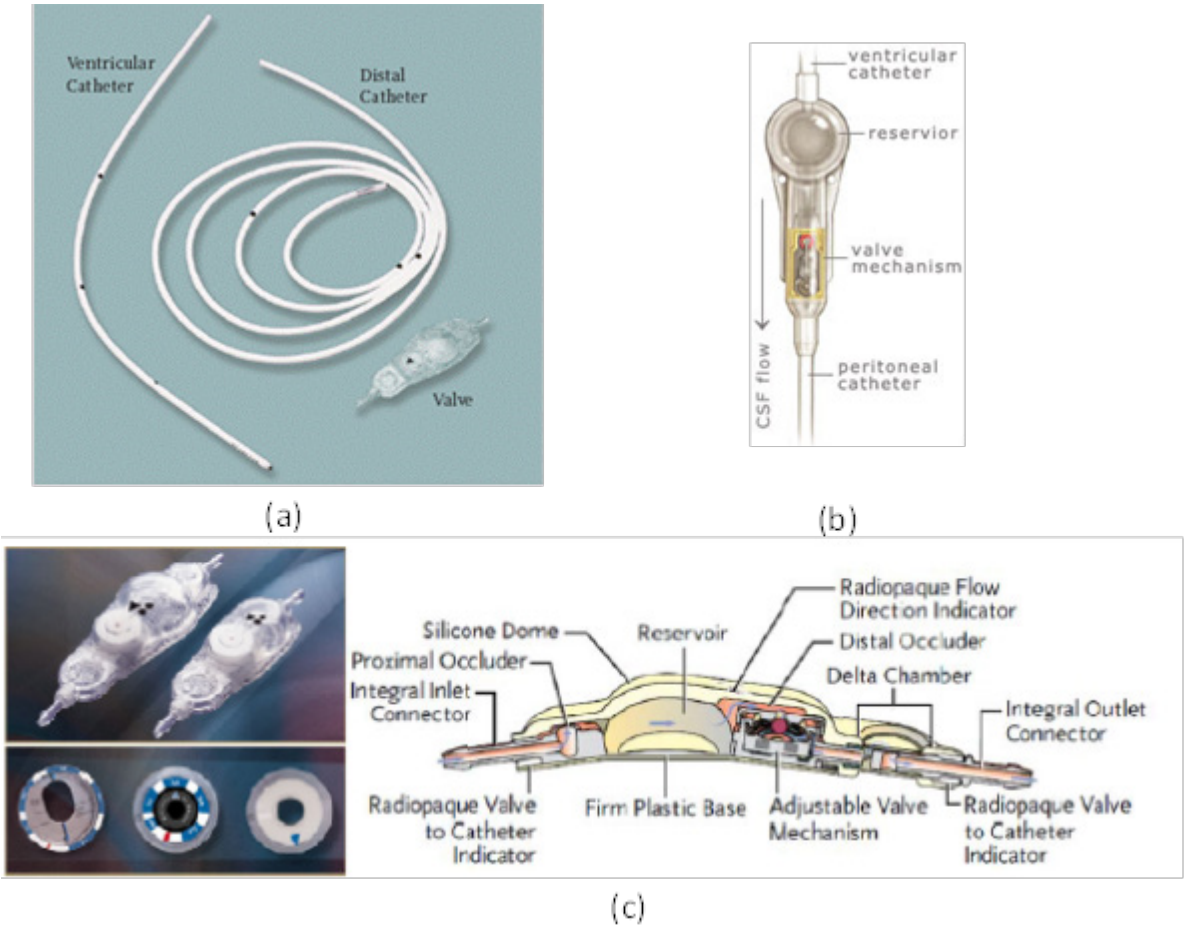

Figure 1.3. A shunt system. (a) Shunt components, (b) & (c) Adjustable valve in detail (www.medtronics.com).

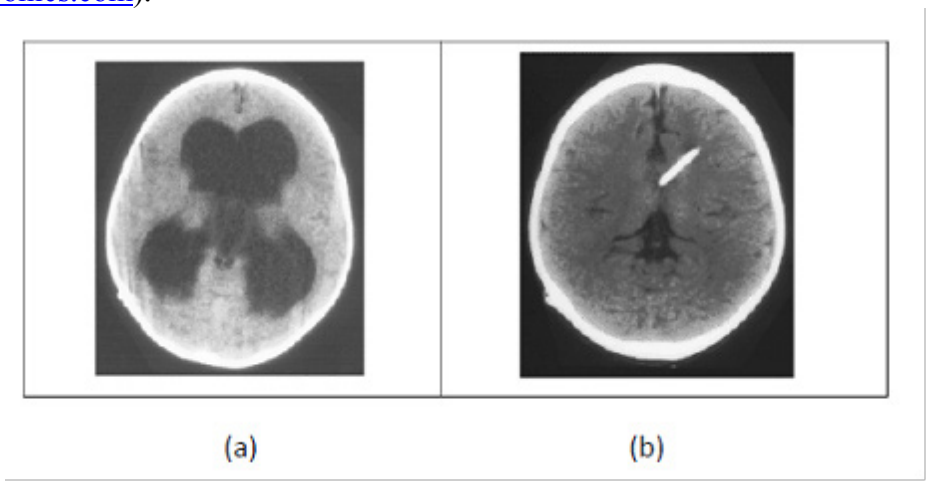

Figure 1.4. CT image of brain (a) before shunt placement (b) after shunt placement (from [29]).

1.3 Shunt Complications

Shunt operation statistics as from the information found from Hydrocephalus Association [4] says there are 40,000 shunt related operations are done in the US every year. That corresponds to more than 100 every day. Shunt operations currently in US cost over 1 million a year and 50% of shunted individuals require a revising operation within two years. One pediatric study found that the average shunt functions for approximately 5.5 years; some shunts require revision much sooner, others later. For an infant under one year of age, the likelihood of shunt revision during the first year is relatively high, approximately 40 percent. Shunt complications may include mechanical failure, infections, obstructions, and the need to lengthen or replace the catheter. Generally, shunt systems require monitoring and regular medical follow up. When complications occur, the shunt system usually requires some type of revision. About 45% of the shunt complication occurs due to obstruction in the shunt or shunt malfunctioning [6]. From [7] the obstruction of flow of CSF is the most common mechanical complication (64%) in shunt is at proximal catheter.

When types of shunt failures were looked over time, the early failures were due to the proximal catheter obstructions and infections and the later stage complications are at the distal catheter. Most of the shunt failures in the adult population occur as a result of occlusion in the distal shunt catheter orifice. The distal catheter tip in the peritoneal cavity is at risk to blockage by fat or proteinaceous debris. The distal catheter may also be stuck between bowel loops or may lie within an intra-abdominal fluid pocket. These will increase outflow resistance of the shunt that may result in slowed CSF flow or florid obstruction [13]. Over-draining or under-

draining are other complications that can occur in the shunt. Over-draining occurs when the shunt allows CSF to drain from the ventricles faster than it is produced. Over-draining can cause the ventricles to collapse, tearing blood vessels. Under-draining occurs when CSF is not removed quickly enough and the symptoms of hydrocephalus recur. Over-drainage and under-drainage of CSF are addressed by adjusting the drainage pressure of the shunt valve if the shunt has an adjustable pressure valve.

At present there is no reliable method to identify the location of the shunt malfunctioning. If there is a complication, the whole shunt needs to be replaced and this is a costly process. A shunt itself costs more than $12,000. If the position of the blockage can be determined, then only that specific part needs to be replaced reducing the complication of the surgery. Determination of flow of CSF can give an indication of over-drainage or under-drainage in the shunt, which can potentially cause other complications. A study to characterize admissions related to ventricular shunts in the year 2000 in terms of diagnoses, procedures in [7], gave the following results from 5574 admissions. The diagnoses treated for shunt malfunction was 40.7%. Age frequency of admissions was non parametric, being highest for infants; the average stay was 8.4 ± 0.2 days. The most common procedures were ventriculoperitoneal shunt placement (43.4%) and ventricular shunt replacement (42.8%). Average cost was $35,816 ± $810. Primary payers primarily were private insurers (43.8%), Medicare (26.0%), and Medicaid (24.5%).

1.4 Prior Works

Over the last 4 decades due to the development in integrated circuit technology and MEMS many medical devices have evolved. These technologies made the devices small and a possibility of implanting more complex devices. Increase in healthcare costs along with longer living population and injuries created a demand for these implanted devices which are wirelessly connected to base stations. MEMS technology has proven to be very successful in reducing size and power consumption as well as possibility of integrating with manufacturing processes used in semiconductors. Miniaturization of sensors provides better integration as well as local measurements. Nearby proximity of the sensor to the quantity measured is of great importance as it provides more accurate measurements and is very important in medical systems. The form factor of the device is much better when the device is battery-less.

1.4.1 Remote Powering and Data Transfer

Modern implementation of wireless power transfer involves two methods: Inductive and radiative. Inductive system uses the principle of magnetic fields to transfer power, which is near field with a range of a few centimeters. When current passes through a coil creates a magnetic field around the coil. The increase in number of loops the coil increases the magnetic field strength. If a second coil of wire is introduced near this magnetic field, a current is induced in the second coil. This works like a transformer without a magnetic core which reduces the efficiency of the power transfer. Devices such as Philips Sonicare [14] tooth brush in Figure 1.5(a) is charged successfully making use of the inductive coupling and thus avoiding the need of routing physical wires. Also the regular electrical connectors can be avoided for charging. Water

can seep in through the connector which can cause damage to the electronic components in the charger. The primary and secondary windings are very close and hence these devices got very high power transfer efficiency. In an electronics tooth brush, the base is connected to the wall outlet which draws a current and it flows through the primary coil in the base producing the magnetic field. If the tooth brush is placed in the base, it induces a current in the secondary coil in the tooth brush, charging the battery. If the distance between primary and secondary coils increases, this method is not efficient. The higher the distance of separation, there is a need for a bigger primary coil with more number of turns. Magnetic field travels in all directions wasting a lot of energy if the field generated by the primary coil is very high. In Figure 1.5(b) and 1.5(c), RF energy harvesting boards from Cymbet and Powercast is shown. The Cymbet board makes use of the RF inductive resonant coupling at 13.56 MHz to recharge a battery in the board. The Powercast board uses RF radiative powering at 915 MHz to transfer power and data.

The clog detection and monitoring system must be implantable along with the shunt. This requires very low power circuit design techniques and the electrical components to be as small as possible. Systems with batteries tend to be bulky and they may cause complications in the surgical procedure. Battery-less powering with on-demand data acquisition is the best approach for these types of design requirements. Without battery, the implanted system has to harvest energy from external sources needed for its operation. Typical energy harvesting sources in the environment are vibration, heat, light, and radio waves. Depending on the operating condition of the system, the available energy from the sources varies. The choice of the energy harvesting source depends on the availability of the source. For example for an implantable system, ambient light cannot be used for energy harvesting. Better choices for energy harvesting for an

implanted systems are heat and radio waves. Another consideration is whether the source will be able to provide sufficient energy for the proper functioning of the system. If the energy harvesting system has low available energy per unit area, it will make the size of the implantable system larger. For our application with the power requirements for the implant, RF resonant powering is best suited. With better circuit components and by lowering the transmission energy using smart protocols, other energy harvesting techniques may become viable in future.

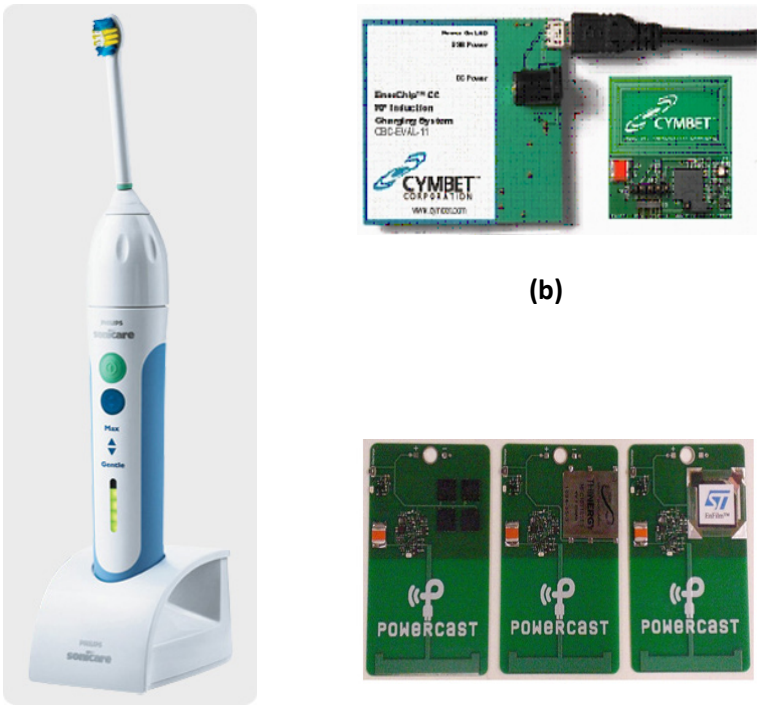

Figure 1.5. Inductive powering examples (a) Philips Sonicare tooth brush (from [38]), (b) Cymbet RF induction charger (from [39]), (c) Powercast RF energy harvester (from [40])

The clog detection and monitoring system must be implantable along with the shunt. This requires very low power circuit design techniques and the electrical components to be as small as possible. System with battery tends to be bulky and they may cause complications in the surgical procedure. Battery-less powering with on-demand data acquisition is the best approach for these types of design requirements. Without battery, the implanted system has to harvest energy from external sources needed for its operation. Typical energy harvesting sources in the environment are vibration, heat, light, and radio waves. Depending on the operating condition of the system, the available energy from the sources varies. The choice of the energy harvesting source depends on the availability of the source. For example for implantable system, ambient light cannot be used for energy harvesting and better choices are heat and radio waves. Next consideration is whether the source will be able to provide sufficient energy for the proper functioning of the system. If the energy harvesting system has low available energy per unit area, it will make the size of the implantable system larger. For our application with the power requirements for the implant, RF resonant powering is best suited. With better circuit components and by lowering the transmission energy using smart protocols, other energy harvesting techniques may become viable in future.

Inductive-coupling based systems as such are not suitable for implantable devices because of low power transfer efficiency and distance. To improve this, resonant inductive powering is mostly used in implantable electronics which improves the power transfer efficiency and the range of transmission. This is technique is used for power transfer but are not often used for data transmission. The resonant inductive coupling like the regular inductive coupling uses two coils. These coils are attached to capacitors and form an LC tank circuit which oscillates at resonant

frequency. If the coils are out of range of each other no energy is transmitted. Also if the resonant frequency of each coil is different no energy is transmitted. If the two coils have the same resonant frequency and are within range of each other, energy is transmitted. Also a coil can send electricity to several other coils as long as they are in range and resonate at the same frequency. This type of energy transfer have stationary field around the coils and no field is spread in all direction as in inductive coupling. This kind of energy transfer is called non-radiative energy transfer and efficiency of power transfer is very high compared to inductive power transfer.

In radiative systems the RF waves transfer energy from the primary coil to secondary coil. They are used primarily for transfer of data in most of the present wireless systems available in market. Energy transfer is not as efficient as the inductive coupling but range is more. Passive RFID tags used for tracking purposes works on the radiative energy transfer principle. For biomedical implant, an inductive link is preferred. The frequency of operation of these systems is in kHz to low MHz range. Optimum frequency for implants is in the low MHz range [15]. High frequencies used in the radiative methods cause more damage to tissues. These tags use backscattering [16] to send data back to the RFID reader. Most of the tags use load modulation for data backscattering. Load modulation is the process by which impedance seen at the reader is modulated by switching off the load. This causes a change of reflected impedance at the reader which is seen as a voltage change at the load switching frequency.

There are other works in the literature that explains about implantable sensors and wireless powering/charging for different applications. In [17] the authors talk about a low-power low-

voltage current readout circuit for inductively powered implant system. The system can detect current in the range of 0.2 μA to 2 μA and generate a waveform whose frequency is proportional to current. They also mention two versions of the circuit in which one uses amplitude-shift-keying (ASK) chip to generate a wave with frequency between 76-500 Hz. The second circuit uses frequency-shift-keying (FSK) signal that generates data between frequencies 1-9 kHz. The FSK based circuit consumes 4 times more power compared to the ASK based circuit.

In [18] Ginggen et al. describes an implantable pressure sensor for long-term monitoring of intracranial pressure. The system uses a capacitive pressure sensor which varies with the pressure and converted into frequency modulated signal by an application specific integrated circuit (ASIC). The sensor is powered wirelessly and can be interrogated wirelessly to obtain the sensor information. The paper also proposes about a novel packaging required for implantable electronics. The sensors and electronics circuits are hermetically packaged in a borosilicate glass chamber where the sensors are exposed to the pressure through a hole in the glass. Most of the MEMS based sensors in the literature are usually packaged by an oxide or nitride layer with a silicone layer on top.

Another inductive link-based wireless power transfer system is presented in [19]. This system consists of an inductive power transfer unit and a backward data transmission unit which uses FSK modulation. Inductive link in the system transmits 125 mW of power with 12.5% link transmission efficiency which is useful in powering most of the implantable units. Another low power integrated pressure sensor system is presented in [20]. Absolute capacitive MEMS based pressure sensor fabrication and system integration is explained in the paper. Another inductive-

link based power and data transfer is mentioned in [21] in which data to the implanted unit is done using amplitude modulation and the communication to the external reader is done using absorption modulation.

There are other works that shows implanted circuit with charging circuits. In one of the relevant works in [22], the authors talk about a mixed signal system for inductive transfer of power and data to an implantable device with the option of charging a battery. The system includes and Li-Ion battery to provide constant power supply for autonomous deployment. The ASIC for the system is designed in 0.35 μm CMOS technology. In another relevant work in [23] authors talk about a wireless chronic bladder pressure sensing device. The implanted system uses two different channels for power and data transfer needing two antennas. A piezoresistive absolute pressure sensor was used for the system which uses a novel offset cancellation techniques are used for maximizing the sensing range of the ADC. The proposed system that we designed face similar challenges the pressure sensors in the implantable system needs to be absolute pressure sensor and there is always the effect of atmospheric pressure in the measurement. This limits the amount of amplification that can be provided to the sensor signals. The atmospheric pressure measured by the sensor is redundant information which does not needed to be amplified. A similar approach can be used in our system for cancelling out the atmospheric pressure before amplification.

1.4.2 Miniaturization of Sensors

The other line of work that is important for the proposed design is the miniaturization of the sensors and incorporates these sensors in a catheter. These concerns are not addressed in the

present work. Some good papers in this field are [24], [25], [26]. In [24] the authors describe a flexible polymer tube integrated with different types of MEMS sensors. Sensors for measuring temperature, flow, glucose concentration are mounted on a flexible planar structure made into a spiral structure as shown in Figure 1.6. The sensors are fabricated with Kapton film as substrate which allows biocompatibility, flexibility and mechanical robustness. A similar approach can be employed for placing the sensors inside the shunt catheters.

In [25] a micromachined differential pressure sensor is explained. There are two separate pressure sensors in the device which can measure pressure and volume flow-rate. The fabrication process used here are silicon and glass processing techniques. These sensors can be used for low cost low power consuming applications but for accurate for flow measurement, additional temperature compensation is required. In [26] a review of development of the micromachined flow over the years is presented.

1.4.3 Research for Smarter Shunt Devices

Shunts were used for the treatment of Hydrocephalus for the last 60 years. There were many advances made in the treatment of Hydrocephalus during this time period. With the significant advances in technology, the treatment of hydrocephalus using shunt has a high failure rate. The complications and the failure of the shunt from these complications are unacceptable. The major advances in the shunting over this period of time are the introduction of antisiphoning devices and programmable valves. These technologies have not lived up to the promise and the failure rate of the shunt remains about 40% within the first 1-2 years. As of the early 1980, the discussion happening in the hydrocephalus community is about improved control of CSF

diversion. The shunt complications mentioned in section 1.3 is not addressed in any of the new generation devices. The currently available valves provide no information about ICP and no other feedback about clog location or self-diagnostic capability. Patient symptoms and interpretation from medical imaging are still used for shunt failure detection.

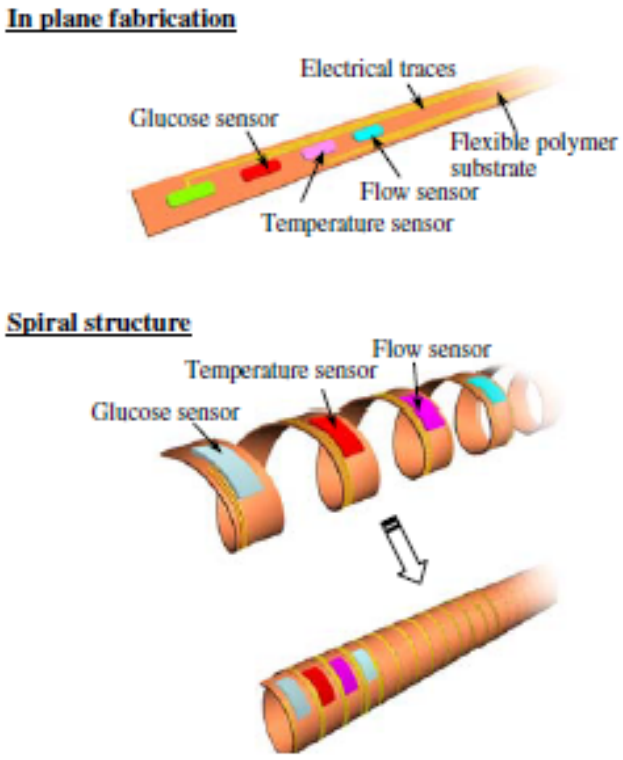

Figure 1.6. Picture depicting the fabrication of the spiral tube with sensor. (from [24])

With major advances in technology over the last 50 years, Hydrocephalus shunts remain relatively unchanged. Ventricular catheter is just designed as a tube with holes sizes arbitrarily chosen as 500 microns as they were manufacturable at that size [32]. There are many varieties of valves in the market with four major manufacturers controlling the market share. They are

Medtronic, Codman, Aesculap, and Integra LifeSciences. Distal tubing is typically marketed as an open silicone tube with 90-120 cm in length.

There are available literatures about researches to make the shunt smarter from 1980's. In 1988 Rekate et al published a proposal for a smart shunt design [33] with CSF flow control. The paper also explains the role of physician in adjustment, hardware size, device size and implant location. Two platforms of the system with battery powering and external powering are described. Unfortunately at that time, the system cannot be realized because of technology limitation. There are many patent literatures from major shunt companies. A feedback control is used on a pump-based smart shunt is described by Medtronic in patents from 2006 to 2008 [34]. In another patent from Medtronic in 2001, it describes about sensor based implantable monitoring system that could be used for valve control [35]. Codman and Shurtleff in a patent in 2012 describe a mechanical valve with a pressure sensor and an actuator replacing the magnetic adjustment mechanism used in the present shunts [36]. The system can be operated under an algorithm or can be controlled by the physician.

Although there is a lot of a research in developing smart shunts, there is no evidence of a complete smart shunt developed. Most of the research is concentrating on a few components needed to make shunts smarter. Most of the designs are in a conceptual level. Many investigations [44], [45] showed changes in posture of the patients induce drastic differences of intra-ventricular hydrokinetic pressure. This pressure difference changes the drainage rate of CSF through shunt. The classical hydrokinetic parameters that are used for the theoretical design are not optimized for the design of the shunts. Some of the hydrokinetic characteristics of the

pathway between ventricular to peritoneal cavity may not have been considered in the design of the current shunt. Integrating sensors in the shunt pathway to monitor hydrokinetic parameters will give more insights into the shunt complications and aid in a better shunt design.

Table 1.1. Researches in smart shunts.

Related Works	Area of research
Rakate et al. [33]	Proposal of a smart shunt with CSF flow control, two way communication, hardware, implant locations etc.
Al-Nuaimy group, [46], [47], [48] University of Liverpool	Data management architectures and decision making frameworks for smart shunts
Leonhardt group [49], [50], [51], [52], [56] Aachen University	Smart shunts and test systems based on pressure feedback control
Cote et al. [53]	Control algorithm based on ICP variation
Yoon et al. [54] Ajou University, Korea	Micropump and pressure sensor design for closed loop control
Thomas et al. [55] NJIT	Obstruction resistant catheter designs
ETH Zurich [57]	Hydrocephalus dynamics and constructing models
Linninger et al [58], [59], [60], [61]	Developing volume sensor
Our work	Wireless multi sensor platform for the detection of location of clog, flow rate monitoring

1.5 Contribution and Organization of this Dissertation

The present day shunt systems are of two types with fixed and adjustable valves. The fixed pressure valves require revision surgery when flow requirement changes. The programmable variable pressure valves such as those from Medtronic [9], Codman [10], and Spiegelberg [11] help to prevent revision surgery due to flow requirement change. The existing shunts still will not give any information of the complication (e.g. clog) if it does occur. Strong motivation for the proposed research comes from the fact that at present there is no reliable method to non-invasively identify the location of the shunt malfunctioning. When there is a shunt obstruction, all the points along the shunt course are suspect during revision [12]. If there is a suspected shunt complication, the whole shunt is often replaced and this is an invasive and costly process. To avoid this, a system that can provide information about flow and the location of the clog is designed. This system, consisting of sensors to measure the flow and pressure inside the shunt, is proposed. We also designed a wireless powering and data transmission for the system. The proposed implanted device is obtains the power required for its operation from an external reader using the principle of RF resonance. The data transmission also occurs through the same inductive link used for power transfer. The sensors require excitation voltage and since these sensors are resistive, they draw current in the range of mA. The technique we used to power only one sensor at a time and using the same amplifier and ADC for signal conditioning all the sensors, helps to reduce the hardware components and calibration procedure.

With the proposed system added to the shunt, the health care professionals will be able to resolve the shunt complications better and hence improving the reliability of the present system. In this work we propose to detect the location of the blockage and identifying the specific part of

the shunt that may need replacement, thus reducing the complication of the surgery and shortening recovery. If there is an obstruction in the shunt, our system can potentially reduce the number of incisions to be made in revision surgery from three to one. Also, we determine the flow rate of CSF that can provide an indication of over-drainage or under-drainage in the shunt, which can potentially cause other complications. Our system monitors ICP and IAP, which can potentially provide underlying condition of the symptoms shown by the patients. The system measures the pressure at various points in the shunt ad different body postures and the system calculates the flow rate at these postures. This information is useful in setting the valve opening pressure in the shunt. Also, the data collected by our monitoring system over period of time provide the medical staff more information about the medical condition of the patient.

Although this work requires expertise in multi-disciplinary areas, this work mainly focus on designing a lab prototype addressing the clog detection and flow measurement with wireless powering and data transfer capability. The contribution of this work involves

1) A methodology of detecting the clog and Flow Measurement and the theory behind it. (Chapter 2)
2) The electronic circuit and system design used for flow measurement and clog detection. (Chapter 3)
3) Prototype development and firmware design (Chapter 4)
4) Methodology and the need for measuring ICP, IAP, posture pressure measurement (Chapter 5)

CHAPTER 2

SHUNT MONITORING METHODOLOGIES

2.1 Clog Detection Methodology

The major objective of this work is the determination of the spatial location of the clog. Flow sensors were initially considered for the work. There is a possibility of no flow CSF through the shunt catheters even if there is no shunt complication. The flow sensor will not be able to identify the location of the block. Thus pressure sensors are chosen for identifying the location of clog. In this work we propose placing multiple pressure sensors on the inside wall of the shunt catheter for clog detection.

In the proposed sensor placements in Figure 2.1, S1 measures the average ICP in the ventricle, S2 just above the programmable valve, S3 is placed below the valve, and S4 is placed at the further end near peritoneal cavity measuring abdominal pressure. The number of sensors determines the precision of the clog location. In the case of four sensors, it splits the shunt in to five regions i) above S1, ii) between S1 and S2, iii) between S2 and S3 (programmable valve) iv) between S3 and S4 and, v) below S4. This approach will get us a spatial resolution of detection of clog to proximal and distal catheter which reduces the complexity of surgery. In general, if there are k pressure sensors, it splits the shunt system to k+1 region which will give us k+1 possible location of clog. With MEMS technology it is possible to add more sensors, but for the

present requirement and the surgical procedure four sensors are sufficient. With more sensors, there are more electrical connections which is a big overhead in an implantable system.

The location of block in the shunt is determined by comparing the recorded pressures at each sensor locations. There are four sensors placed along the direction of the shunt. Two sensors are placed in the proximal catheter and two in the distal catheter as shown in Figure 2.1. Sensors are placed at four locations along the direction of the tube. A prototype system made using an IV container and shunt catheter tubing is used for obtaining the pressure recordings at the four locations. The valve is placed between sensor 2 and sensor 3 to control the flow of liquid.

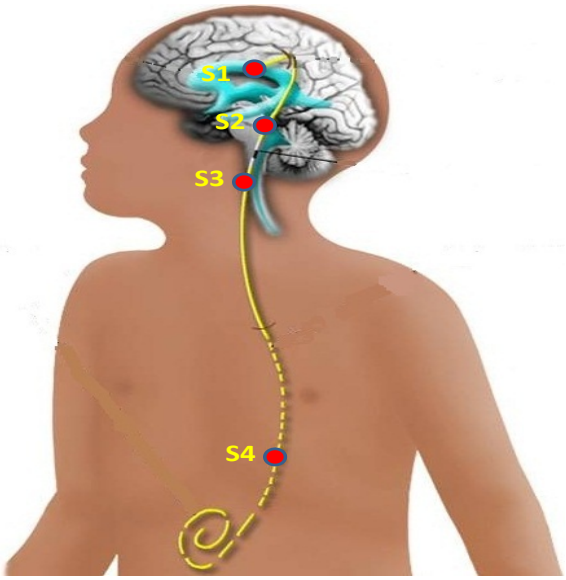

Figure 2.1. Location of pressure sensors in the shunt in the prototype.

According to theory, flow of liquid in a tube produces a drop in pressure between two points along the direction of flow. By measuring pressure at two points, flow rate of the fluid can be determined. When there is an obstruction of flow, the static CSF column in the shunt increases

the stress on the sensors and produces a higher pressure reading. When there is flow, there is a decrease of pressure due to friction. Such pressure change is captured for detecting the location of failure. This method can be employed in the detection of fully obstructed shunt with 100% accuracy. Partial clogs can be detected, but in some cases, it is detected as a fully obstructed clog. This can be improved by increasing the sensitivity of measurement and a better understanding of how the clog develops in the shunt.

2.2 Flow Measurement

The fluid mechanics system used in the prototype works according to Bernoulli's principle. Bernoulli's theorem describes the behavior of a fluid under varying conditions of flow and height and it says the energy at any point in a liquid flowing through the pipe is the same. It is basically the law of conservation of energy. Pressure sensors are used in the shunt to determine the location of clog in the shunt. From the readings from the sensors, flow can be computed using Bernoulli's theorem. In fluid mechanics, *head* is a concept that relates the energy in a fluid to the height of an equivalent static column of that fluid. Head is expressed in units of height such as meters or feet. Head is also fluid's energy per unit weight. Pressure head is due to the static pressure exerted by the fluid on the pipe, velocity head is due to the flow of liquid in the pipe and potential head is due to the height of the fluid relative to a reference point. According to Bernoulli's theorem, the head (H) of the system at any point along the system is the sum of potential head, pressure head and velocity flow head. When the diameter of the pipe is small (in mm), the frictional loss head should be taken into account.

An example of a fluid dynamic system is shown in Figure 2.2 is a pipe system that distributes water from a reservoir. When the valve at a point after P3 is closed, water is filled in the pipe and exerting a static pressure on the valve. Since there is no flow, velocity and frictional head is zero. The head at different points (P1, P2, and P3) must be same and is the sum of potential head and pressure head. The pressure head is measured by the sensor which for no-flow condition is called static pressure head. This static pressure is measured by the sensors placed at different locations along the pipe. The measured pressure will be highest at lowest elevation point in the pipe.

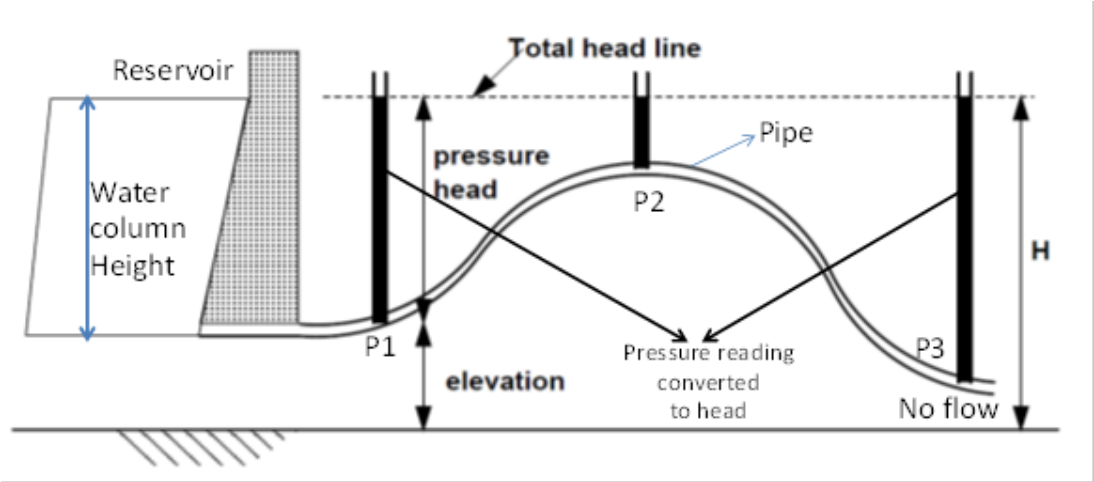

Figure 2.2. Pressure readings taken on the pipe during no-flow. The pressure head is due to the height of liquid column and it is highest at lower elevation.

When the valve is opened, there is flow of liquid. The pressure measured by the sensors drop as they are measuring the static pressure. This drop in pressure is due to the velocity and friction or correspondingly, the loss of pressure head due to velocity flow head and frictional loss head. Frictional loss increases along the length of the pipe. This is clearly visible in Figure 2.3 which depicts the head at three different points along the pipe when there is flow.

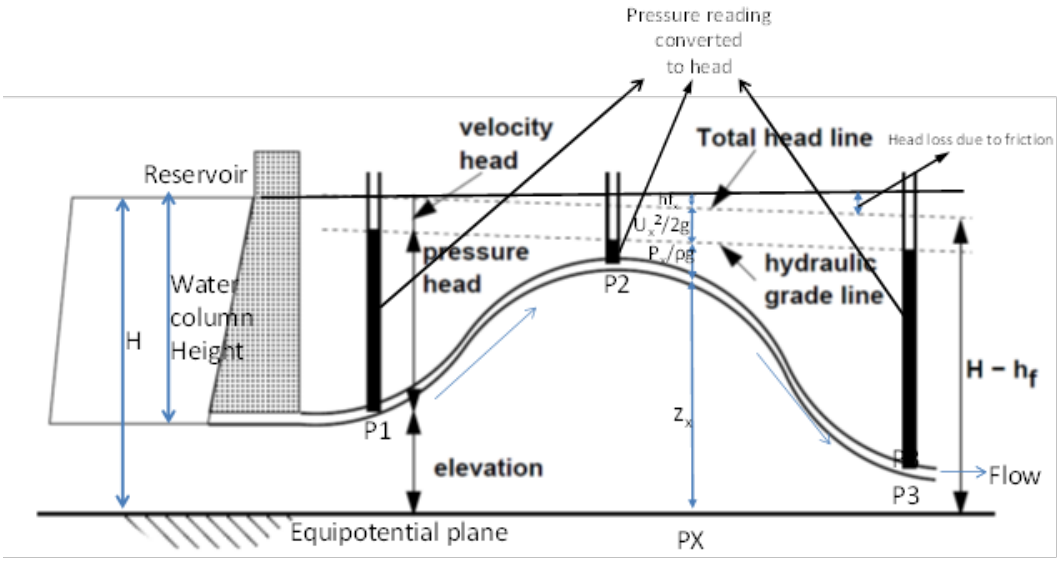

Figure 2.3. Pressure readings taken on the pipe during flow. The pressure head is reduced due to the velocity of flow. Due to friction there is a further loss of head which increases along the length of the pipe.

Bernoulli's equation relating flow for two points in the system in Figure 2.3 is given as

$$\frac{P_1}{\rho g} + \frac{{u_1}^2}{2g} + z_1 + h_{f1} = \frac{P_2}{\rho g} + \frac{{u_2}^2}{2g} + z_2 + h_{f2}$$

where P_1 and P_2 are the pressure at two points along the pipe. u_1, u_2 is the velocity of liquid at those two points. If area of the pipe is same at the two points, then $u_1 = u_2 = u$. z_1 and z_2 are the potential head at these two points from an arbitrary equipotential plane shown in Figure 2.3. h_f is the head loss due to friction. ρ is the density of the fluid. Considering the area of pipe is uniform throughout, the frictional loss between two points in the pipe is proportional to the length of the pipe, and it is zero at the start of the pipe and maximum at the end of the pipe. The sum of all these heads is same in all the flow conditions and along the entire length of the pipe. In Figure 2.4, the total headline indicates the total pressure of the system when the person is standing.

According to Bernoulli's theorem, these must be equal. When there is no flow, the pressure measured by the sensor is the total head line. When there is flow, the frictional loss occurs given by

$$h_f = \left(\frac{64}{2}\right) \frac{Lu\mu}{\rho g D^2}$$

Where μ is the coefficient of viscosity, L is the length of the tube from the beginning of flow, D is the diameter of the tube.

Velocity is found from this drop of pressure due to friction. The Bernoulli's equation can be rewritten for finding the velocity.

$$u = \sqrt{\frac{2gD(\rho g \Delta z - (P_4 - P_3))}{fL}}$$

The following is the steps involved in calculating flow from the measured pressure values.

1. Measure the static pressure difference between the two sensors by having a static liquid column inside the entire tube and let it be ΔP_{static}.
2. Measure the pressure difference between the two sensors when there is liquid flow and let it be ΔP.
3. Find the pressure drop due to friction which is $(\Delta P_{static} - \Delta P)$.
4. Find the velocity of flow from the equation $u = \sqrt{\frac{2gD(\Delta P_{static} - \Delta P)}{fL}}$
5. Calculate the volumetric flow rate using Q= Au, where A is the area of cross section of the pipe.

The potential sources of errors can be due to variation of one or more of the following factors such as the sensitivity of the sensor, amplifier gain, and error in measurement of flow rate. Number of bits of the ADC can be increased for better accuracy. Also if a sensor that can directly measure the frictional loss, velocity can be calculated.

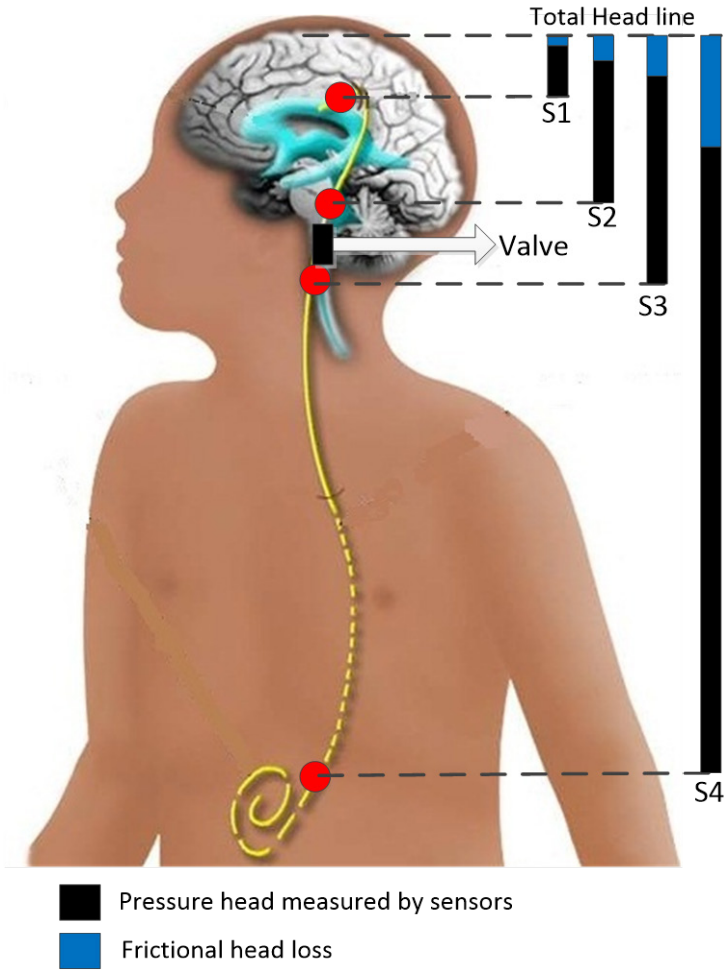

Figure 2.4. The pressure measured by the sensors and the frictional loss.

2.3 Experimental Results

2.3.1 Clog Detection

The measured pressure from the proposed system is shown in Figure 2.5. The system was clogged between sensors S3 and S4 and the pressure measurements were done for a period of 2 minutes at a sample rate of 1. At this condition, all the sensors above the location of the clog will record higher pressure due to the static column of CSF present and S3 records the highest pressure. Sensor S4 will be measuring a lower pressure compared to the other three sensors. When the clog was removed, liquid flows through the tube and the pressure readings of the same sensors are recorded. When there is flow, there is a reduction of pressure readings compared to the clogged condition.

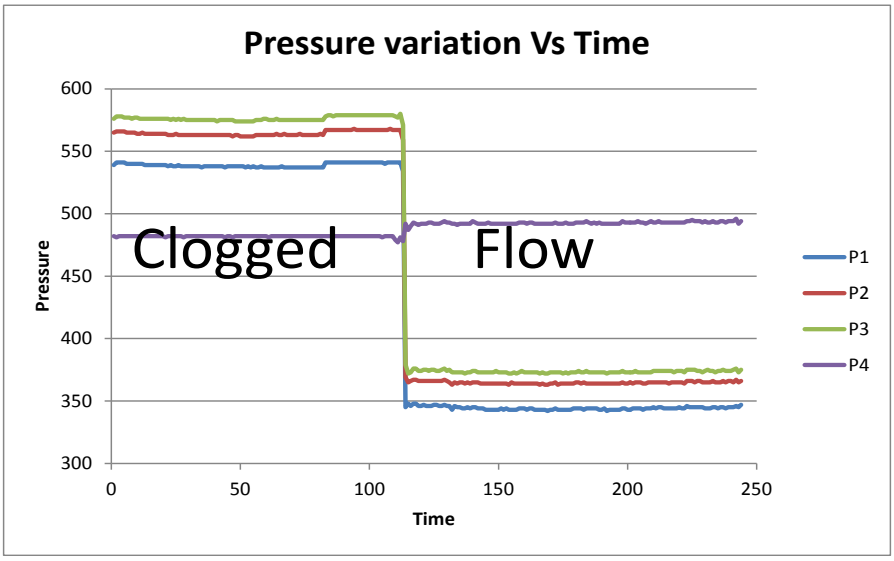

Figure 2.5. Pressure variation of Clogged and unclogged system

Figure 2.6 shows the graph of pressure readings of the four sensors at different scenarios. The region A is for pressure reading when the clog is between S1 and S2, region B for the clog between S2 and S3, region C for a clog between S3 and S4, and region D for a clog after S4. The region E shows the pressure reading of the sensors when there is a liquid flow in the shunt. As it is clearly seen in the graph, in region A, the pressure reading of S1 is high due to the clog below S1. In region B, the pressure on S2 is highest and it is greater than S1 and S1 is greater than the pressure reading of other sensors. In region C the pressure S3 is highest and in region D, the pressure reading of sensor S4 is highest.

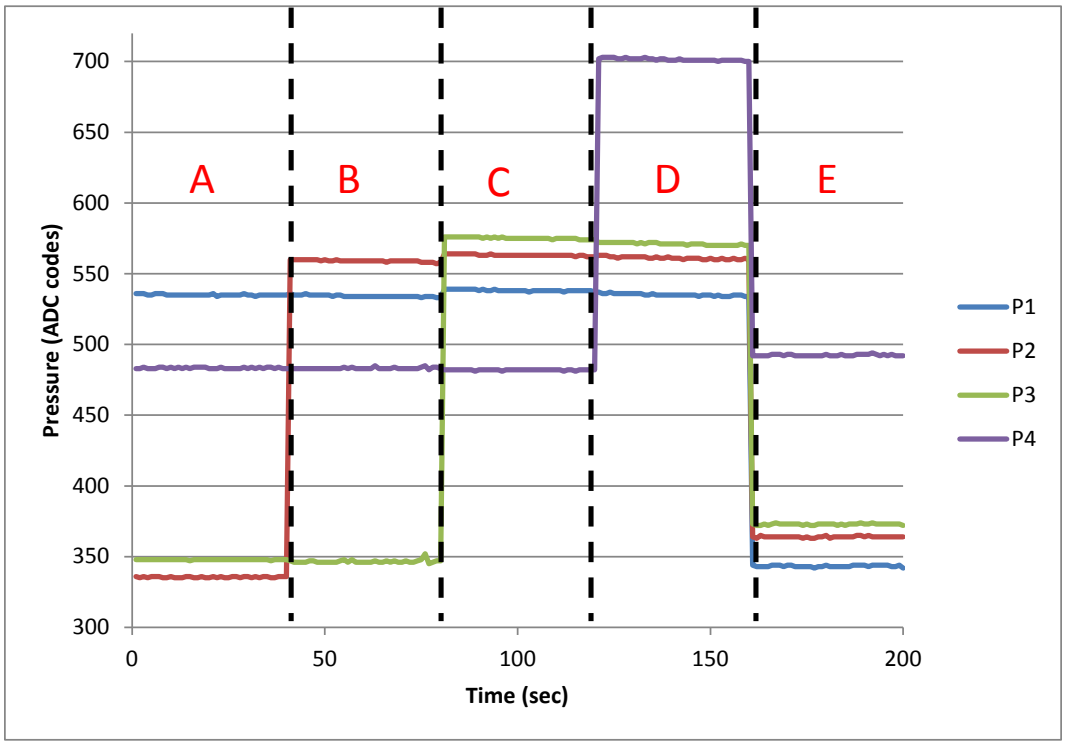

Figure 2.6. Pressure variation of the system with clog at different locations.

2.3.2 Flow rate calculation

Figure 2.7 shows the pressure reading of the sensors at different flow rates. The valve is between S_2 and S_3. At low flow rates, the area at the valve is reduced, so there is a presence of a static water column along with flow and hence high pressure reading on the sensors above the valve compared to higher flow rates. There is also a pressure drop on the sensors below the valve due to lower volume of water and no static column. The measured value of P4-P3 is shown in horizontal y-axis. This value increases as the flow rate is decreased.

In order to find the velocity of flow from the equation, the height difference of S_3 and S_4 should be calculated. This is calculated using the pressure exerted by the static column of liquid on S_3 and S_4 by blocking the tube below S4. By measuring the pressure at the sensor in this condition, the static pressure between S3 and S4 is found out. For the prototype, this height can be measured directly, but in a real shunt, this need to be estimated when patient is at a sitting position. This is very difficult to determine when the shunt is implanted. Since pressure drop due to friction is proportional to the length, it is possible to calculate this value beforehand. When there is a flow of liquid inside the tube, the measured pressure is reduced from the static pressure and this pressure drop is the frictional pressure loss. From the graph in Figure 2.8 it can be seen that at higher flow rate, the pressure drop due to friction is higher and as flow rate decreases, the pressure loss due to friction also reduces. In Figure 2.8, the pressure reading of the sensors P1, P2, P3, and P4 along the primary y-axis and the pressure difference P_4-P_3 in the secondary y-axis. P1, P2, P3, and P4 are the pressure measured by sensors S1, S2, S3, and S4. The

difference between P4 and P3 is taken because the length between these two sensors is the longest and hence more loss due to friction.

The flow rate needs calibration for obtaining good repeatability of the system. This can be done by calibrating the system for various flow rates using an accurate flow meter as reference. The flow is set at a certain value in the flow meter and the sensor pressures are measured at this flow rate for a period of time. Average of this pressure difference between two sensors are calculated and used for the calculation of the flow.

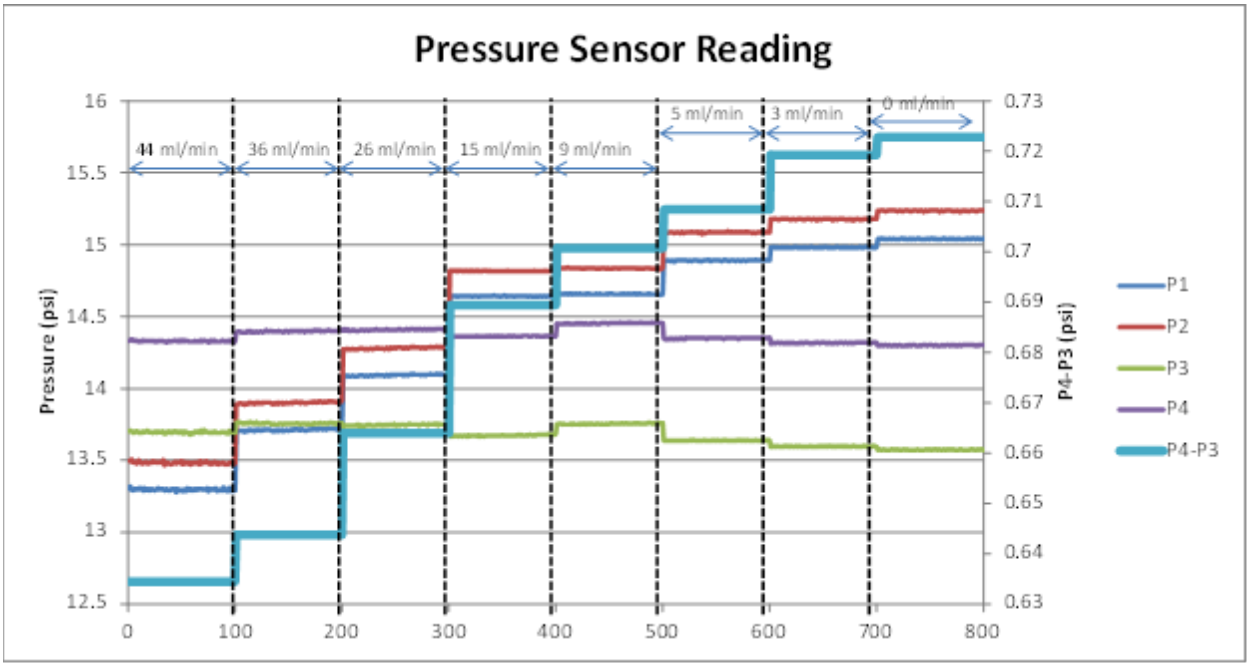

Figure 2.7. Sensor reading for various flow rates when flow control valve is between sensors S2 and S3. P4-P3 is plotted on the secondary y-axis.

Figure 2.9 shows the measured and calculated volumetric flow rates through the shunt at different frictional pressure loss between P4-P3. The flow rates are *measured* using Thomas

scientific 3500 Traceable ultra-low flow meter. This instrument displays the instantaneous flow rate and the total volumetric flow. The instantaneous flow rate is set and the pressure measurements are taken for a period of 10 minutes. The flow rate is measured by taking the average of the volumetric flow displayed by the instrument. The average of the pressure reading for 10 minute period is used to find the *calculated* flow rate. In the real time system, the flow rate is calculated using the average of 20 readings taken at 2 samples per second.

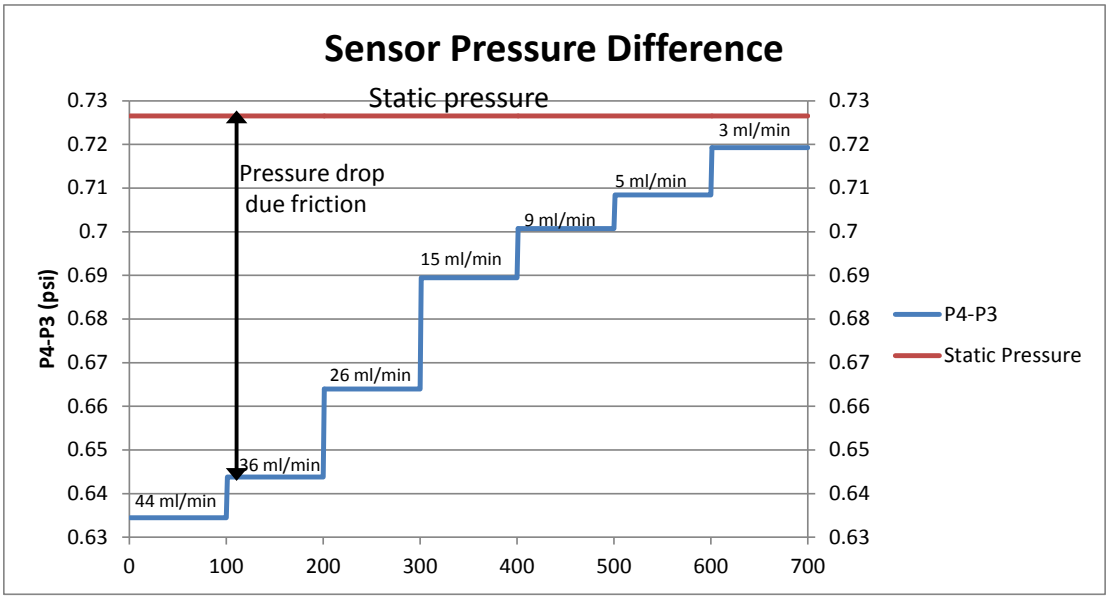

Figure 2.8. Calculated pressure drop due to friction.

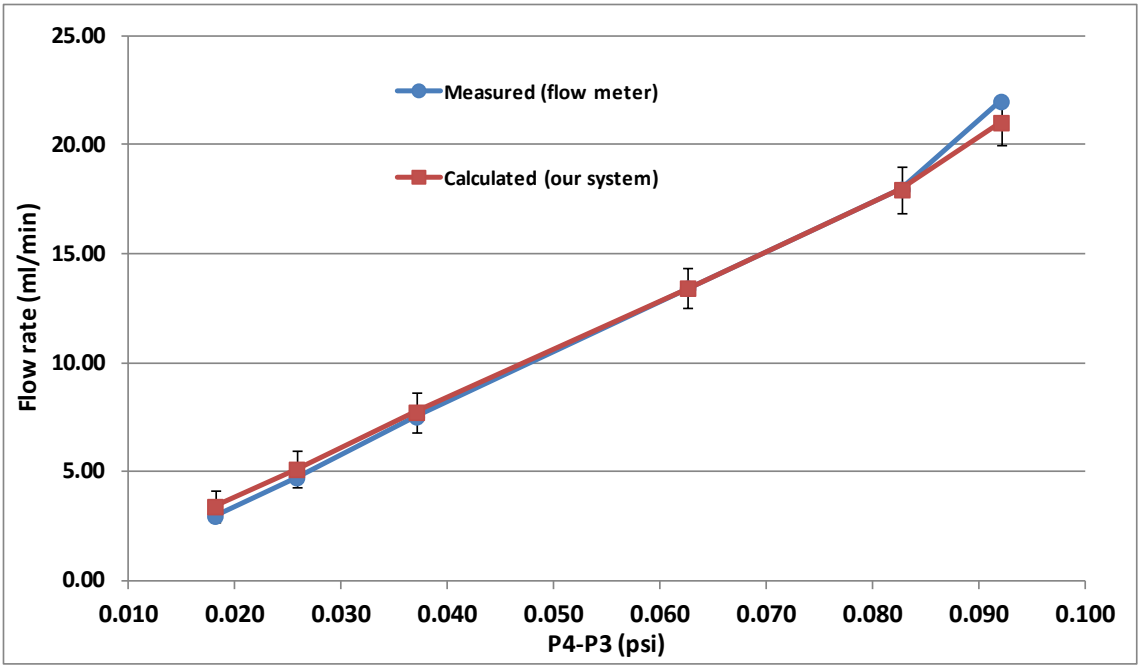

Figure 2.9. Measured and calculated pressure drop.

Table 2.1. Calculated and measured flow rates with percentage of error.

P drop (psi)	Measured (ml/min)	Calculated (ml/min)	Error (%)
0.030	19.6	20.0	-2.2
0.023	15.8	14.9	5.9
0.017	12.0	11.2	6.3
0.013	8.8	8.4	5.1
0.010	6.6	6.4	2.9
0.007	3.5	4.0	-14.4

CHAPTER 3

ELECTRONIC SYSTEM DESIGN

Another major contribution in this work is the design of the prototype system that involves the sensor interface, wireless communication and RF powering. The circuit design concepts and reasons for the selection of the components are explained in this section. There is no off the shelf interface or system that can be directly connected to the sensors for clog detection. The sensors used for the system must be flow-through sensors. Most of the commercial pressure sensors available in the market are not flow-through sensors. These kinds of sensors cannot be used in the application as the CSF will not able to flow out through these sensors.

The circuit for this application needs to be customized as there no inductive coupling system that transmits data and power using the same antenna with required specification. The use of multiple sensors meant the design of a sensor interface that can power sensors in a time multiplexed fashion. Two analog multiplexers (MUX) are used control the power and ground lines to the sensors. The sensors are powered one at a time with a suitable off period before powering the next sensor for proper operation. The output of the sensor is a differential voltage. This voltage must be converted to single ended and must be amplified. This is an analog signal, which must be digitized. An SAR ADC of 10 bit resolution is used for this purpose. The ADC data of four sensors are collected and converted into a data packet and send to the RFIC for modulation.

The system must be able to power the sensors and the sensor interface design as well as the data communication to the reader. The sensors are piezoresistive and they require excitation voltage. So this requires a stable DC excitation voltage and this is provided by the regulator. The constant DC output voltage of the regulator is used for all the components in the design. The sensor interface unit consumes very little current and so does the microcontroller. The majority of power is taken by the sensor and for data transmission.

3.1 System Architecture

The shunt catheter in Figure 3 is about 1 mm in inner diameter with a 0.5 mm thickness. The basic requirement of the sensing system is that it should be able to fit into the current shunt system without affecting its functionality. This means the size of the sensor and the sensor interface circuitry to be minimal along with the capability of powering the circuit and sending the measured data wirelessly. Battery powering makes the system bulky and presents more challenges in the surgical procedure. The block diagram of the proposed system is shown in Figure 3.1. The sensors should be placed in the catheter without any deformation to the original system. This requires the sensor to be MEMS based.

3.2 Shunt Catheter

As explained earlier, the proposed sensor system, the sensors must be placed inside the shunt catheters for the measurement of pressure/flow. Since shunt is a made of sturdy silicone tube which is flexible, once it is inserted in to the body, it is safe to assume the area inside the shunt will not change unless there is a block. In the proposed system, the sensors implanted

should not impede the flow of the CSF. With MEMS sensor, this can be made sure as the thicknesses of these sensors are in the range of a few µm. The miniaturization of the sensors and incorporating the sensors are important aspect for the implantable system, but they are not addressed in this work. Some of the related works about MEMS sensors, hermetic packaging and integrating sensors in to a catheter are explained in [24], [25], [41]. It is important that the packaging and the sensor substrate to be bio-compatible. In the present work, flow-through pressure sensors are attached shunt catheters to measure the pressure.

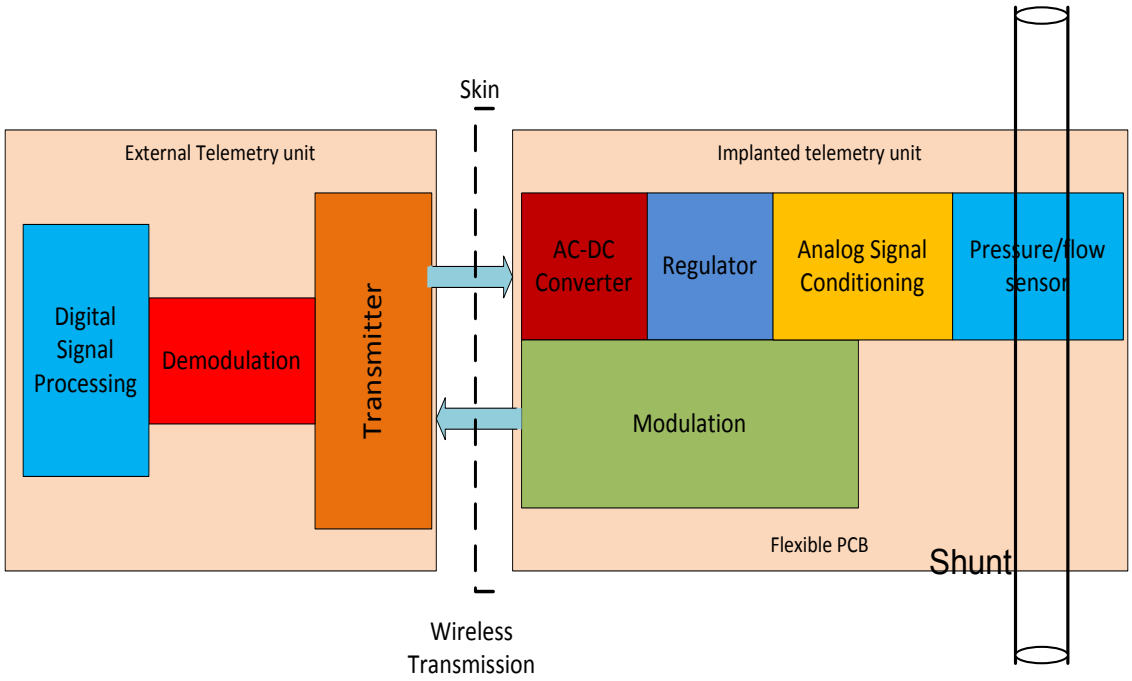

Figure 3.1. Block diagram of the proposed Clog Detection system.

3.3 Sensors

Different pressure sensors are available based on technology, application suitability and cost. There are at least 300 companies making pressure sensors worldwide using over 50 technologies. Most of the silicon pressure sensors are piezoresistive bridges and capacitive sensors. The most popular among them is piezoresistive bridge sensors. When pressure applied to a thin silicon diaphragm present in the sensors, they produce a differential output voltage in response. The piezoresistive pressure sensors are usually made into Wheatstone bridge configuration to capture the change of the resistance to a differential voltage. This requires the application of excitation voltage across the bridge configuration. An excitation voltage VDD is applied as shown in Figure 3.2 and VSS is usually ground potential in a single power supply system.

At nominal condition (e.g. atmospheric pressure) to the sensor, the bridge is balanced or the differential output is zero. The bridge resistors R1, R3 and R2, R4 are arranged on a thin silicon diaphragm such that when pressure is applied, the resistance of R1, R3 increases and R2, R4 decreases. This resistance change unbalances the bridge and produces a differential output signal proportional to the applied pressure value. This output signal is also directly proportional to the applied excitation voltage. Any change in the excitation voltage directly impacts the output signal. At nominal condition, the value of all the resistances is the same and thus the common mode voltage at the output is half the excitation voltage. When a pressure is applied, the Out+ terminal sees an increase in voltage compared to common mode signal and the Out- terminal sees a decrease in voltage compared to common mode voltage. The differential output voltage is

usually very small up to 50 mV full scale. To interface this to an ADC or a microcontroller, the differential output must be amplified into an appropriate range.

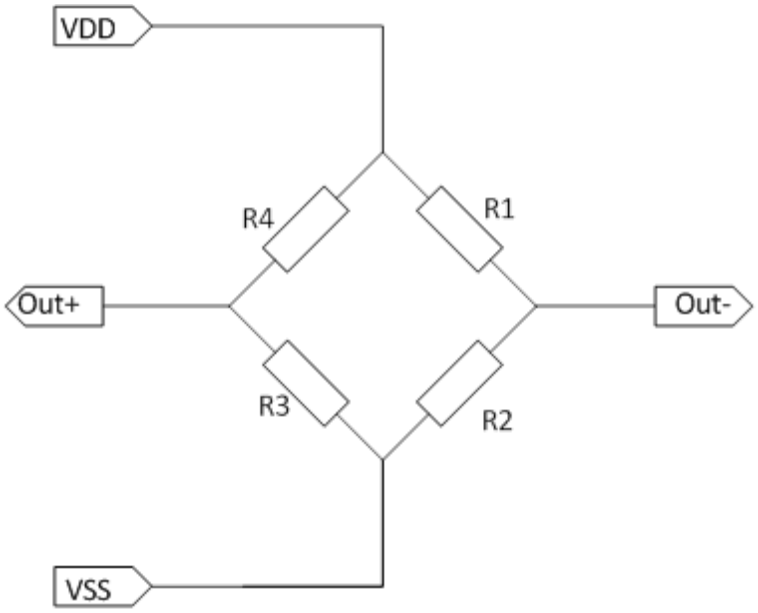

Figure 3.2. Piezoresistive bridge pressure sensors

The sensors used in the prototype are the flow-through gage pressure sensor from Honeywell (26PCAFG6G). These sensors can be added to the shunt catheters inline to measure the pressure at various locations. This sensor the resistors are arranged into a full bridge configuration which has a better sensitivity over the half bridge configuration. It is a full bridge configuration with all the four resistors in the bridge are active sensing elements. The typical sensitivity of the sensor is 1.67 mV/V/psi and typical input impedance is 7.5 kΩ. The excitation current drawn by the sensors at 3.3V is 0.44 mA. The maximum pressure change for this application is about 1 psi or a differential voltage output of 5.5 mV for a 3.3 V excitation.

For the real implantable system, a gage pressure sensor cannot be used for measuring the pressure at various location inside shunt catheter. Gage pressure compares the pressure measured to a reference pressure. In the prototype design, it is the atmospheric pressure. For the implantable system, a reference pressure cannot be provided to the sensors as they are inside the body. Only reference pressure that can be provided is from vacuum. This means that an absolute pressure sensor must be used. With absolute pressure sensors, the sensor voltage output accounts for the atmospheric pressure which comes as an offset. The pressure due to the CSF comes on top of the atmospheric pressure. As the range pressure due to CSF is only about a tenth of atmospheric pressure, this reduces the amount of amplification that can be provided to the sensor. This offset due to atmospheric pressure must be cancelled at the sensor output if the required pressure signal need to be amplified to a better range so that ADC is properly utilized.

3.4 Sensor Calibration

The pressure sensors are calibrated by measuring the offset at atmospheric pressure. The static pressure is measured at different static column of water to get the sensor calibration curve. The calibration coefficients are calculated from the calibration curve. This is stored in the memory when the actual measurements are made.

The calibration curve of S4 is shown in Figure 3.3. A best fit linear line is used to calculate the calibration coefficient. Higher order coefficients can be calculated for a better accuracy, but in the pressure ranges of our application, the calibration curve is almost linear. The calibration curve for each sensor is calculated and the calibration coefficients are reported in Table 3.

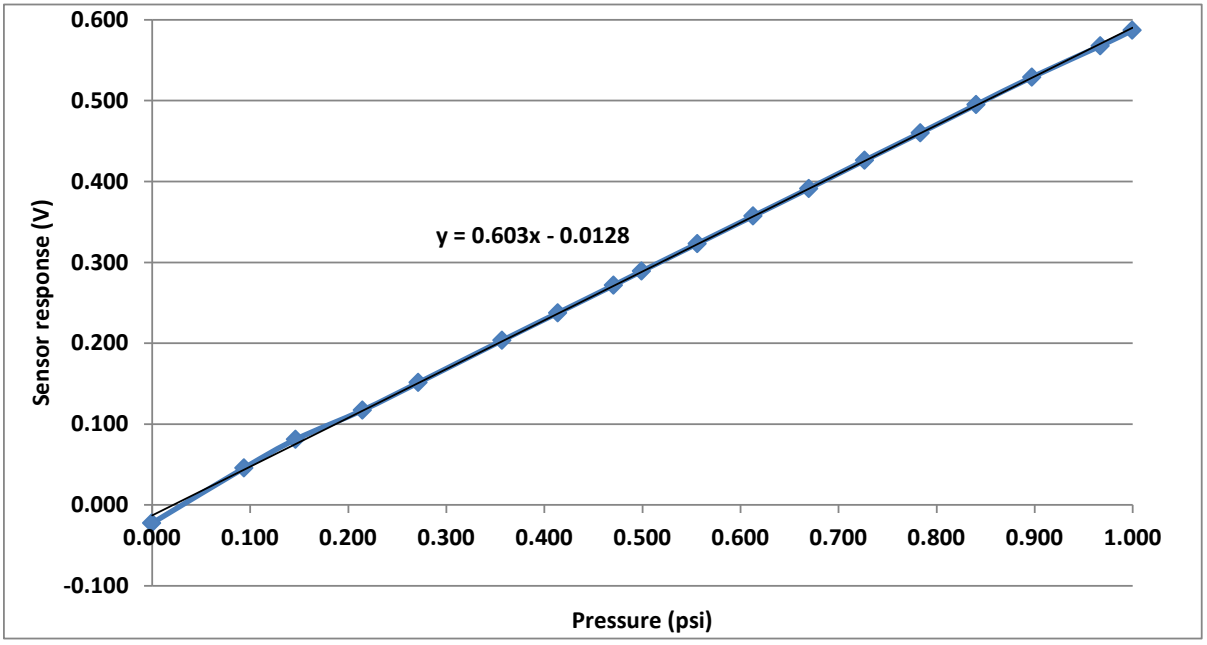

Figure 3.3. Calibration curve for the sensor S4.

The offset of sensors drifts over time. Due to this drift, the sensors need to be calibrated before each measurement cycle. This is impossible if the sensors are implanted as there is no known reference pressure to compare it against. This also means in the implanted system, gage pressure sensors cannot be used. The gage pressure sensor compares the pressure at a point with respect to ambient pressure (usually atmospheric pressure). The pressure near each implanted sensors are unknown and cannot be reliably measured. To avoid this, gage pressure sensors in the present prototype system must be replaced by absolute pressure sensors for implantation.

Table 3.1. Calibration coefficients for all the four sensors

	a_i	b_i
S1	0.594	-0.0093
S2	0.606	-0.0432
S3	0.612	-0.0135
S4	0.603	-0.0128

The possible solution for offset drifts is to measure the sensor pressure at a certain condition (like the valve is totally closed) and calibrate the sensors by recreating the same condition during hospital visits. A calibration method for implantable pressure sensor is mentioned in [28]. In this paper the authors developed an implantable absolute pressure sensor integrated to an undulation pup ventricular assist device (UPVAD). In the calibration process, it is the pressure at the start of the diastolic phase is almost intrathoracic pressure. Intrathoracic pressure is assumed to be close to atmospheric pressure, which is taken for the gage pressure measurement. The authors also mention that this method actually generates an offset error, but since this pressure is always observed at the inflection point, it can be inferred as a zero gage pressure.

3.5 Sensor Interface Components

The sensors used in the system are piezoresistive bridge sensors shown in Figure 20. These sensors need to be supplied with a voltage and the output of the sensor is a differential voltage. The current drawn by the sensor depends on the supply voltage of the sensor and the input impedance of the sensor. The differential sensor output voltage must be conditioned and converted to a digital value and send to an external receiver. Use of battery will make the system bulky and life of the system depends on the battery. When the battery runs out, it needs to be replaced meaning an additional surgery. In order to avoid this condition, wireless powering is proposed. Electromagnetic induction (near-field) is preferred for power transmission due to the minimal impact on the human body compared to electromagnetic radiation (far-field) methods. For better efficiency and a better range than electromagnetic induction, resonant inductive coupling is used.

3.5.1 Instrumentation Amplifier

Piezoresistive bridge sensors provide a slow differential analog signal in the range of a few millivolts. Providing the signal directly to an ADC will not give adequate resolution to the signal. In order to effectively use the range of ADC for the measurement, sensor signal must be amplified. Instrumentation amplifiers (INA) are the most common interface circuits that are used with piezoresistive bridge pressure sensors. Instrumentation amplifier in 3 op-amp configuration in Figure 19 is used for the design. Because of the high input impedance, instrumentation will not load the differential output of the pressure sensor. The required gain can be set using an external resistor R_G. The small differential signal is gained and converted to

single ended with an INA. In order to do that, the differential signal must be subtracted and amplified so that it matches the ADC range. The subtraction process rejects common-mode voltage. In Figure 3.4, the op-amps A1 and A2 provide gain to the differential signal and A3 is the difference amplifier.

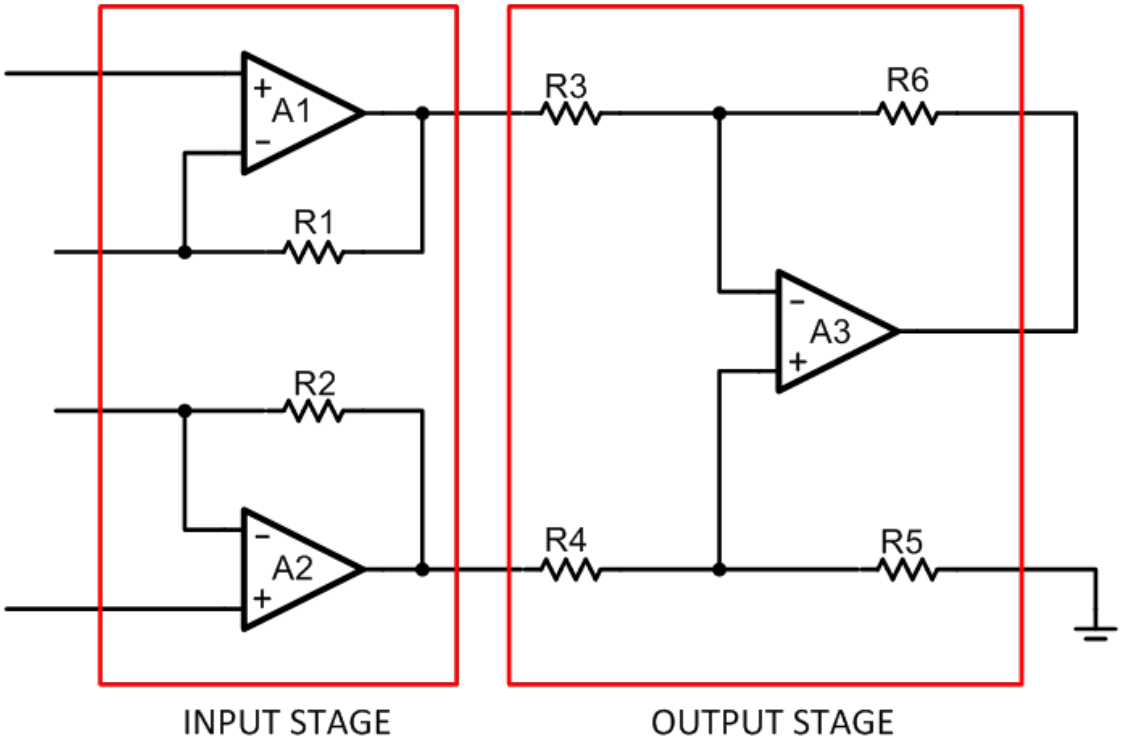

Figure 3.4. Classic 3 op-amp INA. (www.ti.com)

3.5.2 Analog Multiplexers

In the proposed system to measure the clog, multiple pressure sensors are used. All of the sensors used are piezoresistive sensors that require voltage excitation. Powering all sensors at once means increase in power consumption which is not good for implantable system. To avoid this, each sensor are powered one at a time for a few microseconds to complete the measurement

and then isolated from power supply. This is done using an analog multiplexer. A 4×1 MUX is used for this purpose.

3.5.3 Filtering

The sensors had to be routed to the sensor interface board as they are in the catheter. These wires capture 60 Hz power signal which causes changes in the measurement. These are removed by using a low pass filter with a cut-off frequency of 10 Hz. Filter is achieved using a simple RC filter.

3.5.4 Analog to Digital Converting

The amplified signal must be converted to a digital signal for sending to the reader. An external ADC or an ADC in a microcontroller can be used for this. The data from the sensors are converted into required packets and transmitted to the reader using the chosen protocol.

3.6 Sensor Interface Circuit

The sensor interface circuit is shown in Figure 3.5 consists of components mentioned in section 3.5. As mentioned there the output of the sensors is a differential voltage. To amplify the differential sensor output signal, an instrumentation amplifier from analog devices (AD8236) is used. The gain of the amplifier is set at 100 using the gain setting resistors. The current consumption of this device is 0.06 mA and it is in micro small outline package (MSOP). The device has a very small foot print that saves board space and power consumption is very low. It also works from 1.8 V to 3.6 V supply voltage. With the option of working at 1.8 V makes it ideal to use with low voltage components and the possibility of a 1.8 V excitation to the sensor

thereby reducing the power consumption although this method was not employed due to the minimum voltage requirement to the microcontroller is 2.7 V.

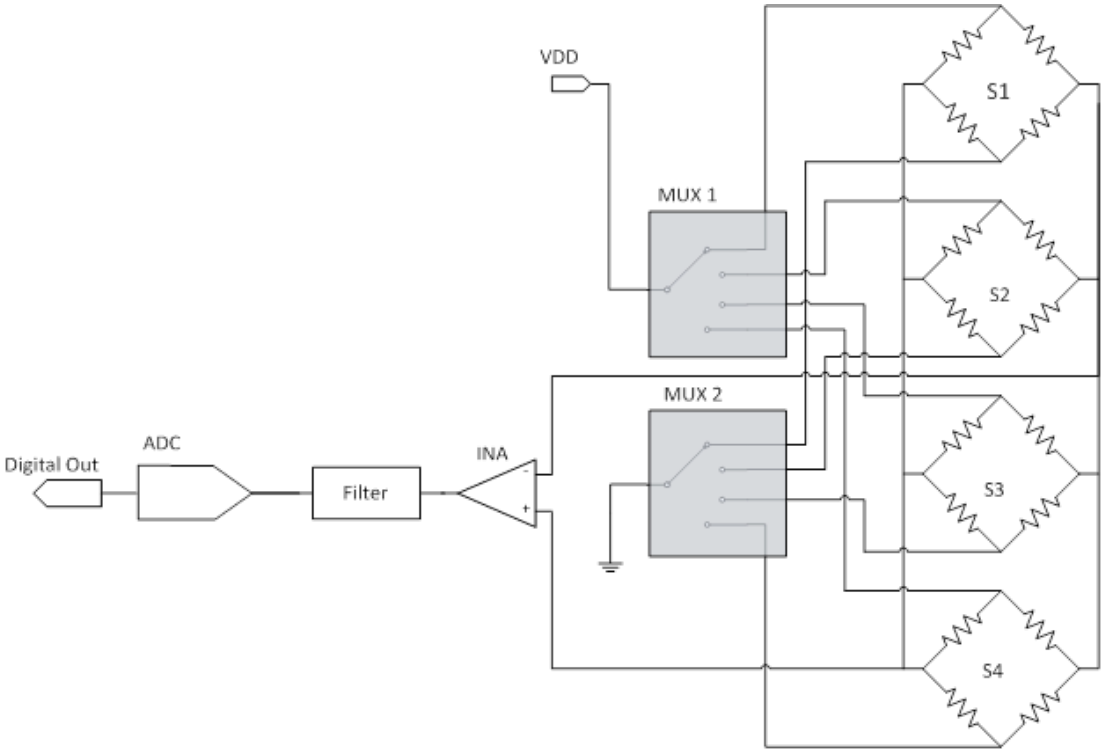

Figure 3.5. Sensor interface circuit.

Two 4×1 analog multiplexers also from analog devices are used to provide VDD and GND signal to sensors one at a time. The multiplexers are controlled by the MSP430 microcontroller. The sensor powering is optimized in such a way that once the ADC stored the sensor value, power to the sensors is cut off and the next sensor is powered. This is continued until all sensors data are stored in the memory. The sensor interface circuit is turned off after all the sensor data are obtained. Signals generated from two I/O pin of MSP430 are used to control the MUX. The 2 control pins for the MUX A0 and A1 shown in Figure 3.6, which controls the 4 MUX outputs

and this, makes sure each Sensor VDD and GND are isolated. Thus only one amplifier is needed for all the sensor amplification. Thus only one offset cancellation and calibration is done for the INA. For the differential pressure measurement, there is no need to consider the offset introduced by the amplifier as the same offset is subtracted from both reading. The only offset now comes from the pressure sensors and the voltage drop in the connecting wires.

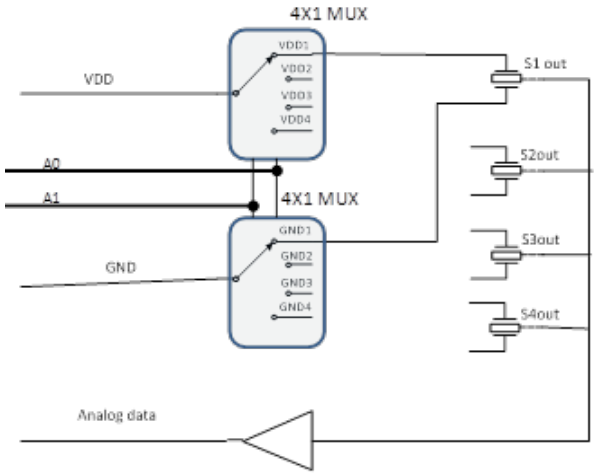

Figure 3.6. The analog MUX control and functionality.

CHAPTER 4

PROTOTYPE DEVELOPMENT

4.1 Clog Detection System using EZ430-TMS37157

The sensor interface design shown in Figure 4.1 connected to a data acquisition system successfully detected the location clog in the shunt catheter. The next challenge is to design a system that wirelessly transfers the sensor data to a PC with an option for power harvesting. A system was designed using an off the shelf development kit EZ430 TMS37157 from Texas Instruments (TI) is shown in Figure 4.1. It consists of an RFID reader which is connected to a PC and a transponder board.

The RFID transponder unit contains a low frequency (LF) RFID transponder IC TMS37157 and an MSP430F2274 microcontroller (μC). TMS37157 receives commands from the reader via the transponder coil which is communicated to the μC via I^2C interface. The sensor data is digitized and communicate back to TMS37157, which modulates the sensor data and sends it back to the reader.

The RFID reader device consists of a LF reader IC TMS3705 and a USB Interface. The GUI commands the target board via reader to instigate the sensor measurement. After the completion of measurement, the reader IC demodulates the received data and sends it to a PC via USB interface or store in memory in a standalone operation. The sensor readings are filtered from the data packet. The GUI displays the location of clog, flow rate, and a real-time graph of

the pressure values. There is an option to save the data into a spreadsheet file for further (e.g. long-term) analysis.

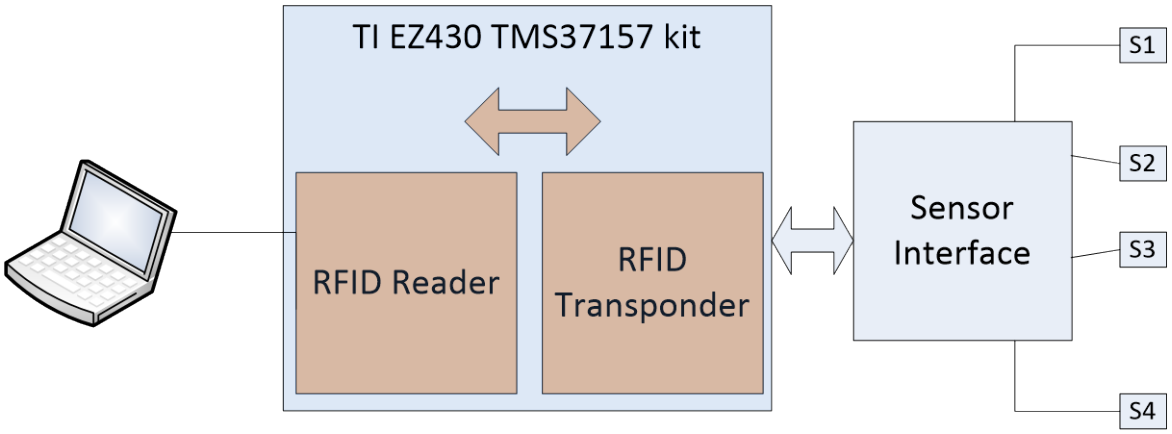

Figure 4.1. Block Diagram of the system with EZ430 TMS37157.

The data from the target board is transmitted to base station. The reader decodes the data and sent the data back to the PC using USB. The Graphical user interface (GUI) gets the data packet from the reader device. Source code of the graphical user interface is in Visual C++. The interface is modified in Visual Studio 2010. The useful sensor information is filtered from the data packet. For pressure sensors, the pressure values of the adjacent sensors are used to calculate the pressure gradient and flow rate. The GUI shows the pressure readings from multiple sensors displayed in the GUI. This data is used to determine the location of clog and display the location as shown in the screen shot in Figure 4.2. This GUI also displays a real-time graph of the pressure values. There is an option to save the data into a .csv file so that it can be used for further analysis.

A picture of the first version of the system with all the components is shown in Figure 4.3. Due to the power required for the sensor interface and the complications in firmware development a custom made transponder was designed using the same RFIC chip used in EZ430 TMS37157 which is explained in the next section.

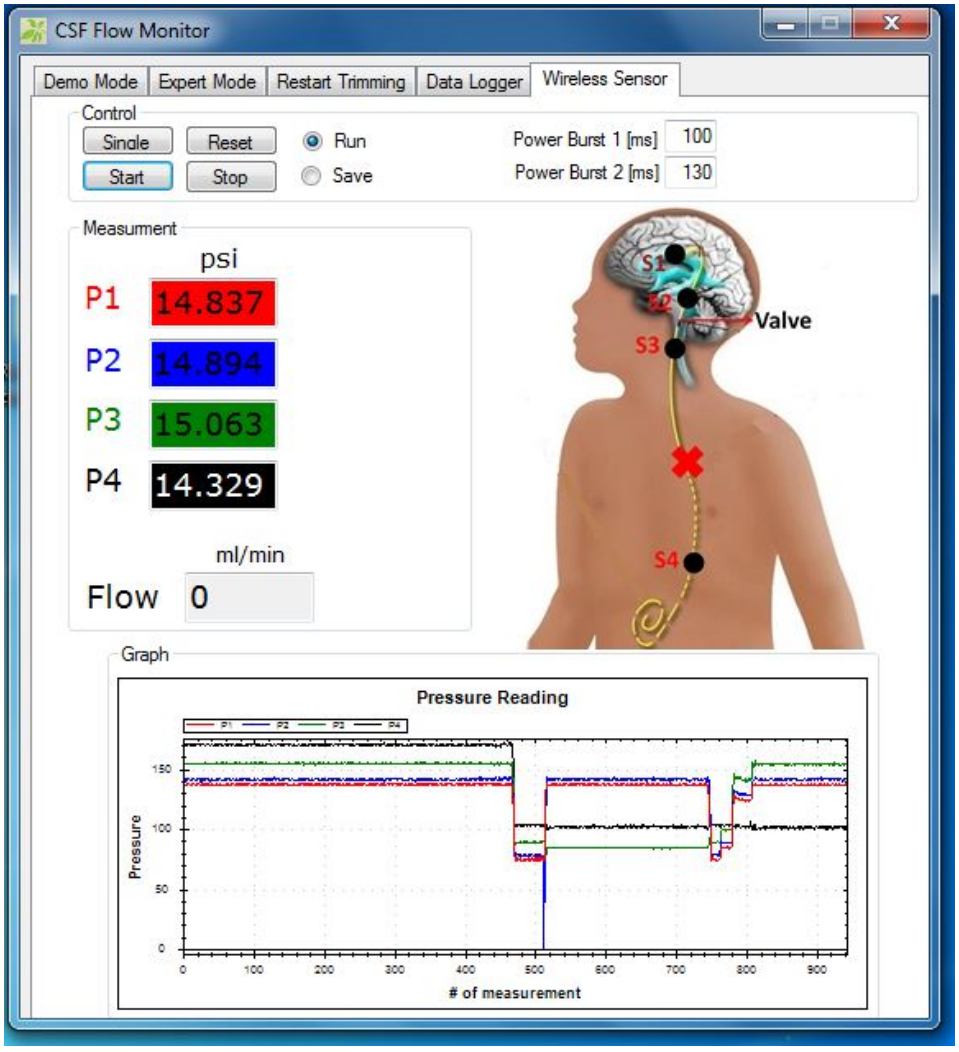

Figure 4.2. Screenshot of the GUI.

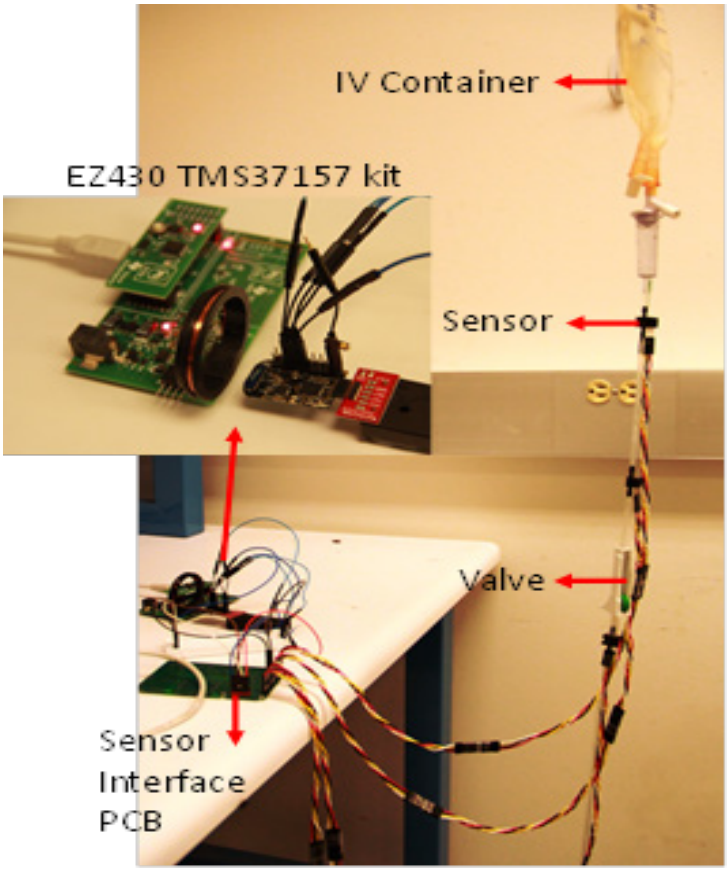

Figure 4.3. A picture of the lab prototype system.

4.2 Transponder Circuit

The transponder circuit for the implanted system in Figure 4.4 consists of the power harvesting circuit, the modulation/demodulation circuit, the data acquisition and the sensor interface. The sensor interface circuit is explained in the above section. In this section the discussion is about the power harvesting, modulation and data acquisition using the microcontroller. The power harvesting is done using the LC tank circuit connected to a regulator. The regulator provides the voltage to all the circuit components. The TMS37157 does the modulation and demodulation functions. The chip communicates with a microcontroller via

SPI with the demodulated signal from the reader. The microcontroller acquires the sensor data and creates packets with the required RFID protocol and sends it to the TMS37157. This data is modulated and sent back to the reader.

In the implanted telemetry unit, at the LC resonant tank circuit, an alternating waveform at resonant frequency is obtained. This signal is rectified and then regulated to get the DC supply voltage. This supply voltage is used to power the sensor and sensor interface circuits. To power all sensors at the same time requires more power and thus need for larger size spiral inductors in the implant unit. To avoid this, sensors are powered one at a time. A microcontroller MSP430F2274 is used to control a multiplexer to power sensors one at a time. The sensor output is amplified and fed to the ADC input of the microcontroller and stored in the memory. The process is repeated to get all the sensor values in the memory. The microcontroller generates frequency signals corresponding to ADC values and this frequency signal is used to generate impedance changes seen by the external inductor (antenna). All the ADC values from the sensors are converted to frequency one after another and the load seen at the implant unit is switched according to the frequency of each sensor in a time shared fashion.

The external telemetry unit consists of a resonant LC tank which is driven by a power amplifier. When the load changes in the implanted resonant circuit, it is reflected back to external resonant circuit and this change is captured to determine the pressure sensor values.

The circuit diagram of the entire transponder side is shown in Figure 4.4. The circuit consists of a resonant tank circuit tuned to 134.2 kHz, a TMS37157 transponder chip from Texas Instruments (TI), an MSP430 microcontroller and the sensor interface. The power required for all these devices are harvested from the RF waves and a regulator connected to the rectified signal to provide a constant 3.3 V to all the components. The TMS37157 is a passive low frequency transponder interface. This interface has a wide voltage range of 2 V to 3.6 V with a power down mode of 60 nA and an active mode maximum of 150 μA. There is a 3-wire SPI interface for exchanging the data with a microcontroller. The downlink is through amplitude shift keying and the uplink through frequency shift keying.

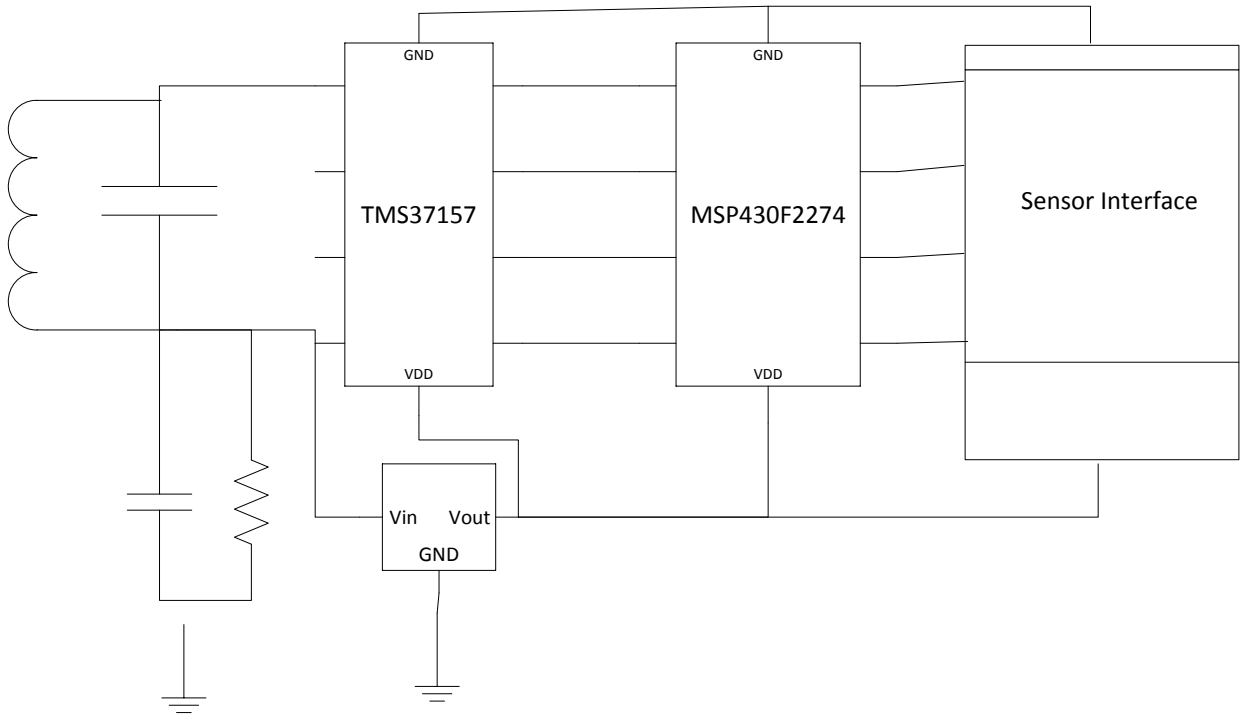

Figure 4.4. Transponder circuit.

4.3 RF Resonant Powering

To power using RF waves over near field (distance of few cm) inductive powering is used. To maximize range and efficiency, resonant coupling is used. In resonant coupling, the resonant frequency of the tank circuit in the reader as well as transponder is designed to be the same or in other words, the product of L and C of the tank circuit is made the same. In Figure 4.5 L1 represents the inductance of the antenna. Size of the reader antenna is made bigger for more power transfer and range. The range of the antenna increases with increase in diameter of the antenna. Capacitor C1 is used to tune the resonant frequency of the tank circuit to the required value which for our system is 134.2 kHz. The capacitor C1 can be connected in series or parallel depending on the demodulation scheme used to retrieve the data.

For maximum efficiency and range, it is important to tune the tank circuit in the transponder to 134.2 kHz. The inductance of the transponder antenna is L2 and the capacitor value is C2. L2 and C2 are connected in parallel so that at resonance, the impedance of the circuit is infinite and thus acting as a current source for load.

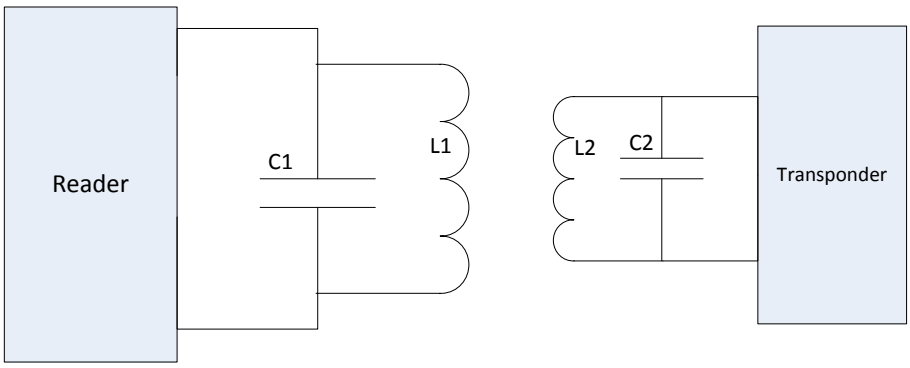

Figure 4.5. Resonant powering of the transponder by the reader.

The LF communication uses 134.2 kHz to transmit data through the inductive link. The resonant frequency of the LC tank circuit is given by

$$F_{res} = \frac{1}{2\pi\sqrt{LC}},$$

where L is the inductance of the inductor and C is the capacitance of the capacitor in the tank circuit. Choosing a transponder coil with an inductor value of 2.38 mH (L2), the capacitor required to make the tank circuit oscillate at 134.2 kHz is 592 pF. A standard value for capacitor available near this value is 560 pF (C2). The exact 134.2 kHz frequency is obtained by tuning the trim capacitor in the TMS37157 IC. The pin configuration of the TMS37157 is shown in Figure 4.6. The IC comes in QFN package. The pin RF1 and VCL is where the tank circuit is connected. The signal from VCL is taken to the input of the regulator.

4.4 Data Transfer

The packet send from MSP430 to TMS37157 is based on the RFID protocol. After the protocol bits, the amount of data that can be send in a package is 6 bytes. For the purpose of clog detection, the resolution of the measurement is not that significant. So for transmitting readings of 4 sensors, the sensor data is truncated into 8 bits (1 byte). For the flow measurement and ICP measurement, higher resolution data is transmitted.

The data transfer to the reader uses FM. There are 16 RF cycles to transmit a bit. The low bit frequency is 134.7 kHz and high bit frequency is 123.7 kHz. This means that it takes 118.8 μs to transmit a low (zero) bit and 129.3 μs to transmit a high (one) bit. This FM principle used is shown in Figure 4.8.

The packets are transmitted to the TMS37157 via SPI. The interface between the TMS37157 and MSP430F2274 is shown in Figure 4.7. The pin BUSY indicates when TMS37157 is ready to receive data from the MSP430 and pin PUSH is used to wake up the TMS37157 from standby mode so that MSP430 can access EEPROM of TMS37157.

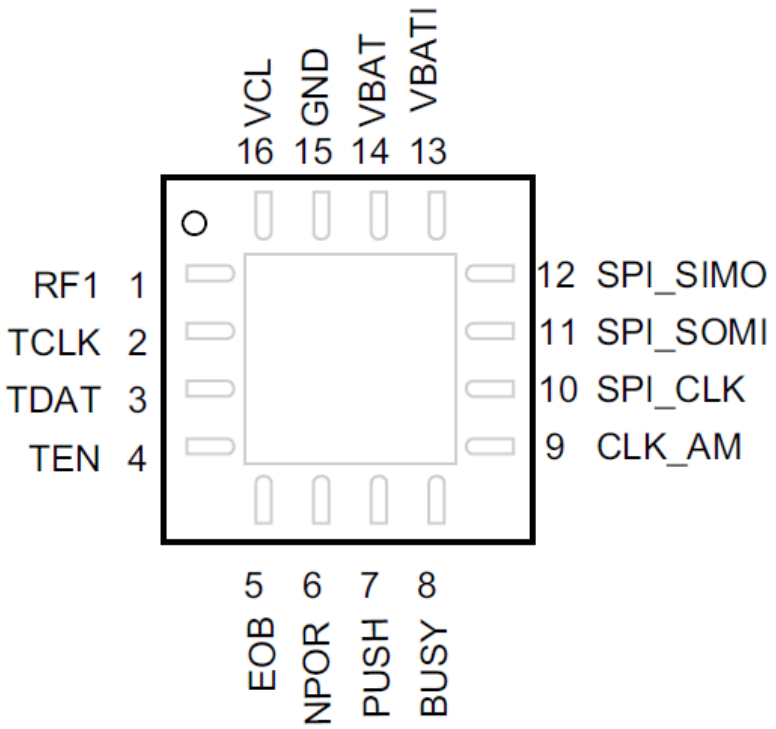

Figure 4.6. TMS37157 pin diagram.

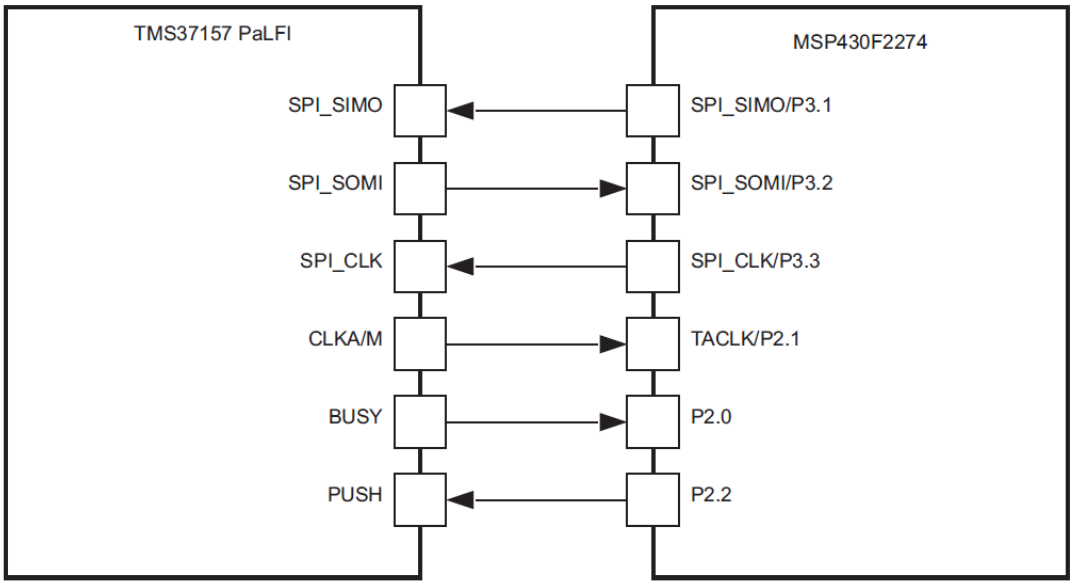

Figure 4.7. Block diagram showing the interface between MSP430F2274 and TMS37157 (www.ti.com).

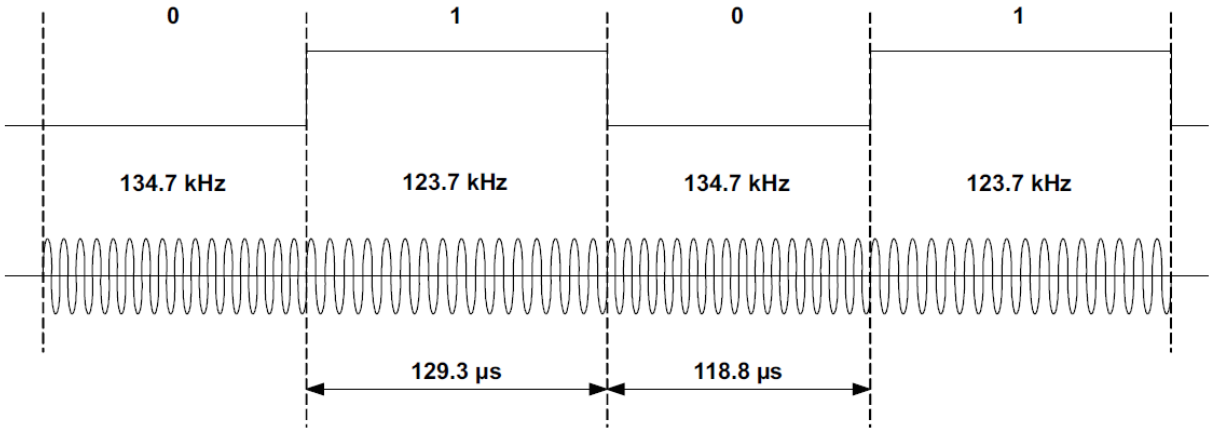

Figure 4.8. FM principle used for transmitting data from TMS37157 (www.ti.com).

4.5 MSP430F2274

The MSP430F2274 is an ultra-low-power microcontroller from Texas Instruments. They have different sets of peripherals including a 10 bit ADC, a 16-bit timer, two op-amps, a universal serial communication interface, and 32 I/O pins. The functional block diagram is shown in Figure 4.9.

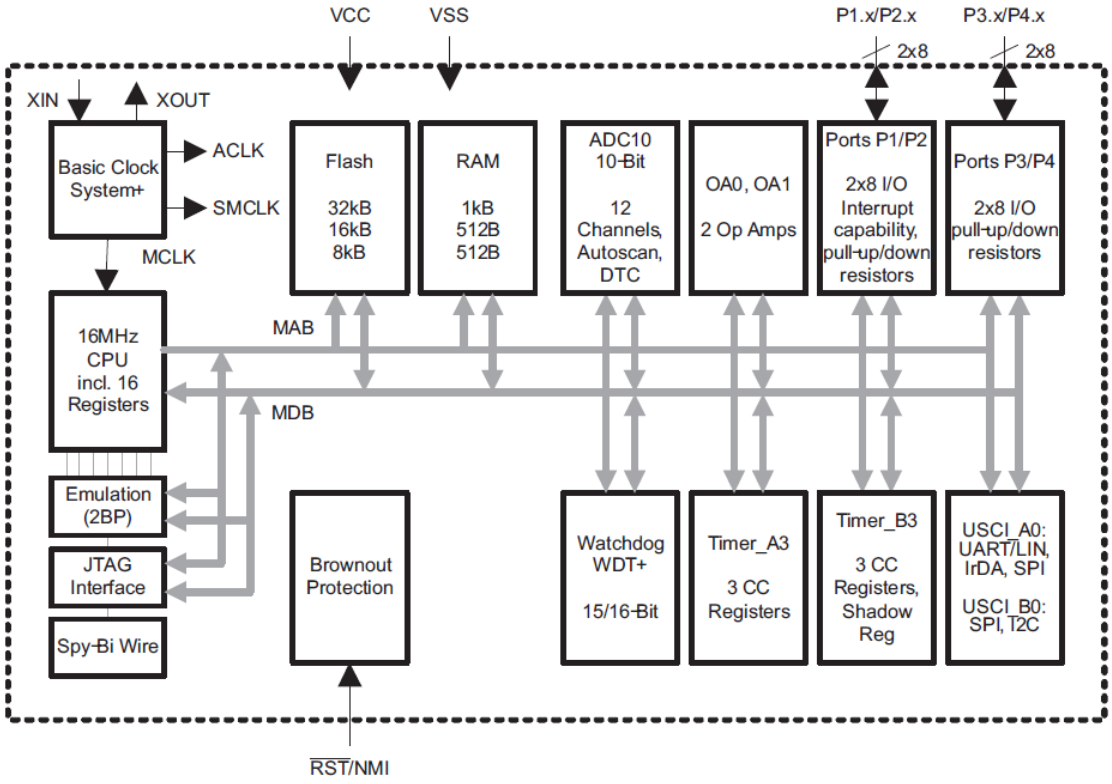

Figure 4.9. Functional block diagram of MSP430F2274 (From www.ti.com)

The main functions of the MSP430F2274 in the transponder circuit are to communicate with the TMS37157 and to control the sensor interface. When the microcontroller is reset and then initialized, it initiates the SPI communication. Then it clears the interrupt flags and enables it

again. It looks for active interrupts, and depending on the interrupt, it performs a specified routine. For our design, the routine is MSP access during BUSY interrupt. During the BUSY interrupt, SPI communication is activated and the MSP430 reads the access data from TMS37157 after that SPI is deactivated. Then the sensor measurement is initialized. The MSP430 generates the control signals to control the sensors. The sensor values are stored in the memory. SPI is activated again to send the data to TMS37157 and the SPI is deactivated. The data acquisition by the MSP430 is given below.

1) Check for proper power at the rectifier output. If power is good, generate the control signals for the multiplexers and the power signal for the sensors.
2) With using proper hold time for the ADC, the sample the sensor output when it is stable.
3) Store the ADC value in the memory.
4) Look for the end of conversion flag. At this time power off the sensor by switching the control signals.
5) Power the next sensor and follow the previous steps.
6) Once all sensor readings are obtained, turn off the ADC.
7) Data packets are filled by one byte at a time. Each sensor data is 10 bits. So the first 8 bits are separated first and placed in the packet and the MSB's are placed in the next slot. In this way all the sensor data is placed in the packet.
8) The data packet is send to TMS37157 for transmission.
9) The entire cycle is repeated again.

CHAPTER 5

BEYOND CLOG DETECTION AND FLOW MEASUREMENT

The complications from shunting are mostly due to failure of shunts. Better understanding of the hydrokinetic parameters and the CSF will help to design better shunts. Monitoring of flow rate, ICP, IAP after shunt implant can help to optimize the drain rate of CSF. Strong motivation for the proposed research comes from the fact that the failure rate of shunt at the present day is very high. Also monitoring ICP will give more insights into hydrocephalus, which can further aid the treatment. When complications occur, the shunt requires some type of revision usually shunt replacement which is a costly process. By getting more pressure data from different locations in the shunt will help in design of better shunt devices for treatment of hydrocephalus.

ICP and other parameters differ from person to person. Another motivation for monitoring ICP, IAP and drain rate is that shunt performance can be optimized and personalized for any particular patient by the surgeon. The key contribution in this work is the design of a prototype system that determines the location of clog, flow measurement and pressure measurement at key locations in a hydrocephalus shunt.

5.1 Intracranial Pressure

Intracranial pressure (ICP) is the resultant of the circulation of cerebrospinal fluid (CSF) and cerebral blood. In general ICP monitoring is useful in the treatment of Hydrocephalus. Specifically the information extracted from the ICP waveform is very useful. This extracted information includes cerebral perfusion pressure (CPP), regulation of cerebral blood flow and volume, CSF absorption capacity, brain compensatory reserve, and content of vasogenic events [27]. The diagnosis and subsequent monitoring of the shunt function for hydrocephalus is aided by the CSF dynamic tests.

In our proposed system, the position of sensor S1 is in the ventricles thereby measuring the real ICP and hence avoiding the problem from measuring the CSF column height at the lumbar. If the pressure transducers are inserted into the ventricle, it not generally re-zeroed at the start of each measurement. For long term monitoring this can produce a considerable zero drift and thus false reading.

5.1.1 ICP measurement techniques

The present methods of measuring ICP are mostly invasive. A transducer is usually needed for accurate monitoring of ICP. The apparatus in Figure 5.1 includes an intraventricular drain connected to an external pressure transducer. The transducer is calibrated externally (Zeroing) and the ICP can be controlled by draining the CSF. The real ICP is ventricular CSF pressure. The pressure inside brain compartments (different ventricles and brain parenchyma) might be different. The pressure measured by most common intraparanchymal probes may not represent the real ICP as the pressure may be compartmentalized. Assessment of craniospinal dynamics

from the lumbar CSF pressure is more often used in hydrocephalus. This method should involve recording of pressure and pulse amplitude for a period of at least half an hour. The CSF pressure measured by height of the CSF column at the lumbar may be misleading as CSF pressure varies over time.

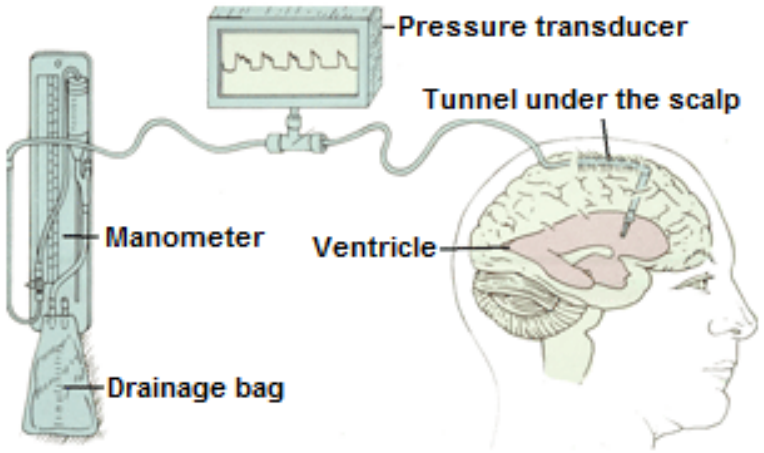

Figure 5.1. Apparatus for an invasive transducer for the measurement of ICP [from [28]]

5.1.2 ICP Value Ranges

The ICP value depends on age, body posture and clinical conditions, so it is difficult to establish a standard value. Normal ICP in healthy adult in a horizontal (e.g. lying in bed) position is in the range of 7-15 mmHg. In vertical (sitting, standing) position, it is negative with average around -10 mm Hg and not exceeding -15 mm Hg. An ICP above 15 mmHg in horizontal position can be regarded as elevated in hydrocephalus.

The ICP waveform consists of three major components in time domain which can be separated to frequency domain as shown in Figure 5.2. These are: (i) slow waves, (ii) respiratory

waves and (iii) pulse waves. The pulse waves have the frequency of the heart and it consists of many harmonics. The amplitude of the fundamental frequency component is very useful in the evaluation of various indices.

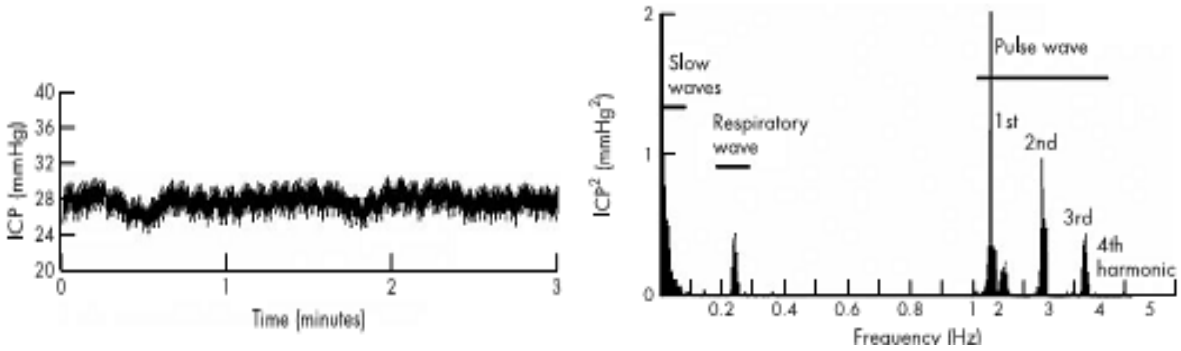

(a) (b)

Figure 5.2. (a) ICP wave form recording (from [1]) and (b) the frequency domain representation of the waveform

To monitor the pulsatile nature of the ICP, the sensor data must be sampled at a rate more than 20 samples per second. To achieve that, after the measurement is initiated, the pressure data is recorded at 64 samples per second and saved into internal memory. Only after the required number of samples is collected, data is sent back to the reader. For the clog detection and flow measurement, once all the four sensor measurements are completed, data is sent back to the reader. This method has a very low sampling rate of 2 samples per second and it will not capture the pulsatile nature of ICP. IAP monitoring is also important for hydrocephalus patients. As the IAP changes at different body postures, the monitoring of IAP can be significant in setting the drain rate of CSF. Also the value of measured IAP might help to determine the migration of shunt catheter. The IAP is also recorded at 64 samples per second due to multiplexing strategy employed in our system.

The flow-through pressure sensor S1 (in Figure 2.1) in the prototype system measures ICP. The pulsatile nature of ICP only occurs in the brain. During the pulsatile motion, the net flow is zero. The effect of pulsatile wave will change the flow rate slightly. This change is captured by the sensor S1. The sensors used in the lab prototype are commercially available flow through sensors. A pulsatile waveform was created by manually turning a valve on and off periodically at approximately 1.5 Hz. The sensor output is sampled at 64 samples per second. The pressure captured by the sensors is shown in Figure 5.3(a). In order to test the response of the sensor, the frequency of turning off and on is increased and decreased by a small amount. This change of frequency is captured by the sensors and it is seen in the FFT of the waveform (peaks at around 1.5 Hz). The fundamental frequency of this manually created pulsatile waveform is captured in the FFT in Figure 5.3(b) along with the small increase in frequency. Pulse waveform analysis of ICP based on power spectrum evaluation was done as demonstrated in [25]. The amplitude of the pulse waveform can be used to estimate cerebral blood volume. The compliance of the brain is correlated to modulation of pulse waveform by respiratory waveform. To capture this amplitude properly, the sensor must be placed on the outside wall of the proximal catheter in direct contact with the pulsatile wave.

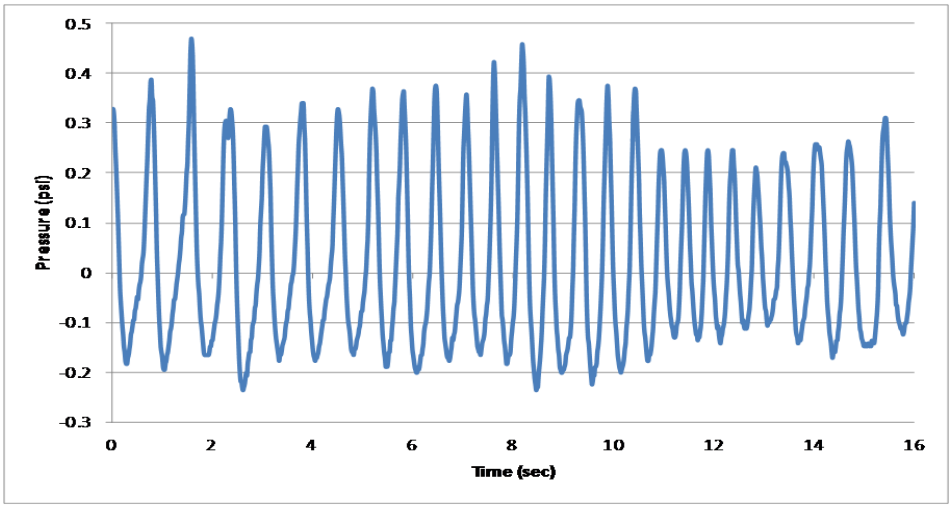

(a)

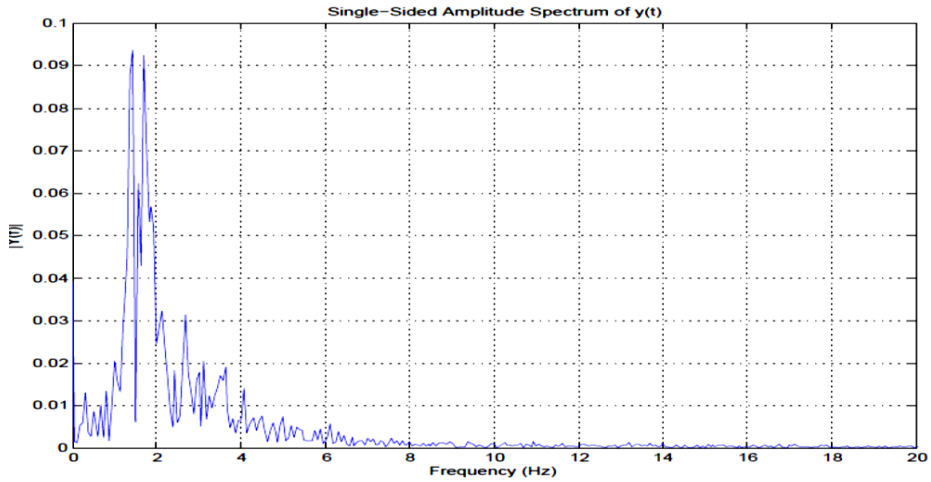

(b)

Figure 5.3. (a) Pressure recorded by S1 from a simulated pulsatile flow, (b) FFT of the recorded pressure

5.2 Effects of posture on clog detection and flow rate measurement

It is also important to measure the pressure at different shunt locations at different body postures like sitting, lying down etc. A model of the system is shown in Figure 5.4 when the patient is in supine position. When a patient is sitting/standing as shown in Figure 5.5, there is an additional hydrostatic pressure (HP) added to the fluid dynamics. This causes an increase in flow rate. The perfusion pressure (PP) is the driving force for CSF. The pressure at the brain ventricle is ICP and there is the valve connected from proximal to distal catheter which has an opening pressure (OP) and then there is abdominal pressure (AP). When the person is standing up, there is an additional hydrostatic pressure (HP). At supine (lying back) position

PP = ICP – (OP+AP)

At standing position

PP = ICP +HP – (OP+AP)

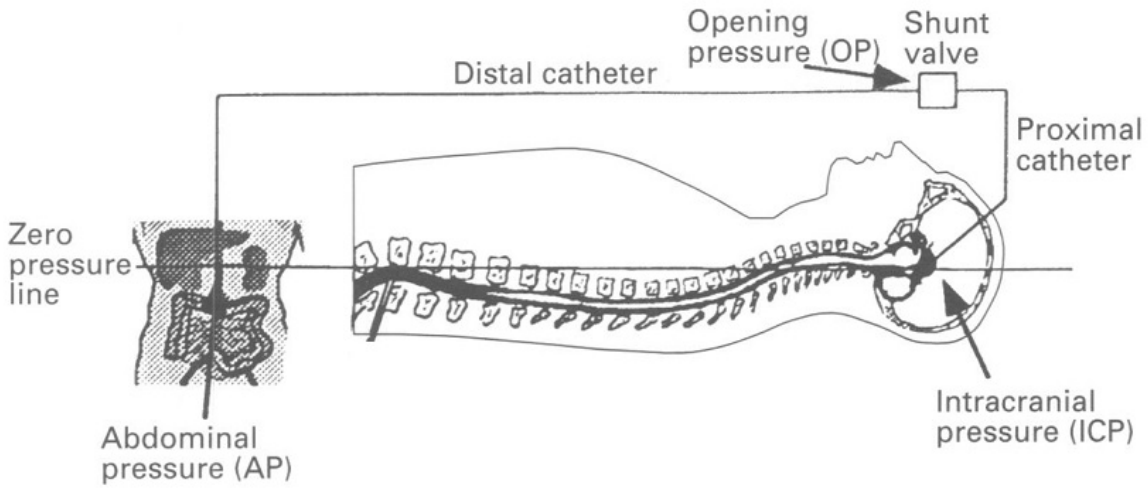

Figure 5.4. CSF dynamic pressure at various points along the shunt in supine position (from [30]).

The pressure measurement of sensors S3 and S4 in horizontal position is shown in Figure 5.6. The pressure is measured when there is a clog after S4 and when there is a liquid flow. For the condition for clog after S4, the pressure readings of the sensors are almost the same and it is very difficult to find out which value is higher. Also when the patient is lying down, if the position of sensor S4 is below S3 in this condition, S3 readings will be higher compared to S4. This will produce false clog detection. When there is CSF flow, the pressure difference between the two sensors is increased as seen in Figure 5.6. This pressure drop is directly proportional to frictional pressure loss and flow rate is calculated from this.

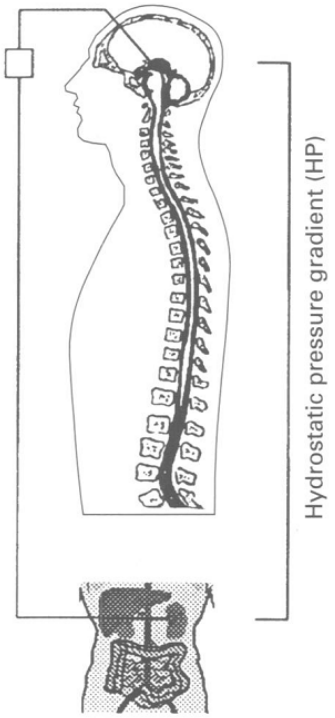

Figure 5.5. CSF dynamic pressure at various points along the shunt in standing position (from [30]).

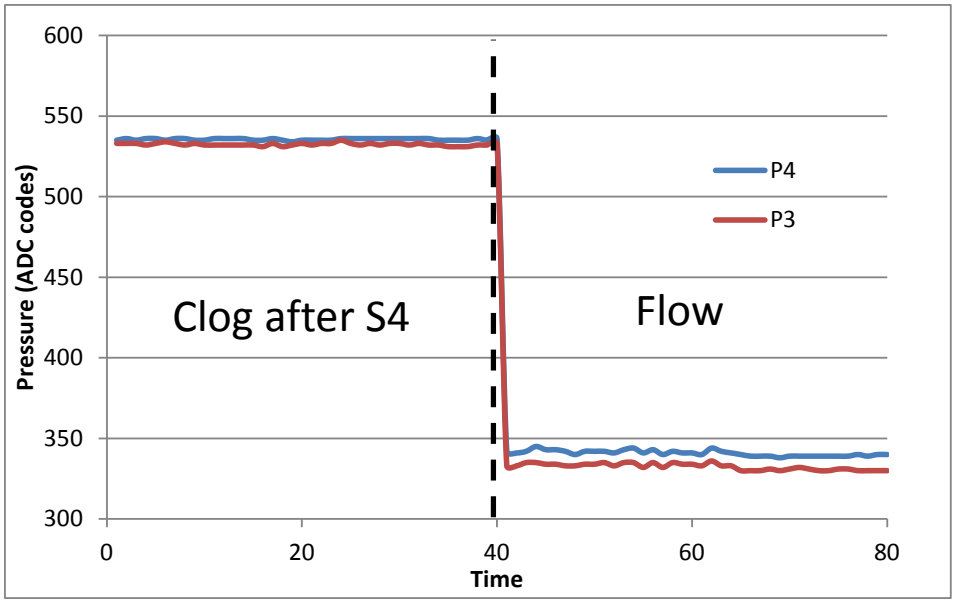

Figure 5.6. The pressure reading of sensor S4 and S3 in horizontal position.

Figure 5.7 shows the pressure reading of sensors S3 and S4 at horizontal position and vertical position for maximum flow rate and no flow condition. This information can be used for online calibration if the flow rate is known. Due to the hydrostatic pressure in the vertical position, the flow rate is higher. The maximum flow rate for vertical position is 20 ml/min and for horizontal position is 16 ml/min. The higher pressure reading on the sensor P4 is due to the hydrostatic pressure of liquid column present in the tube. At horizontal position, there is no hydrostatic pressure present as shown in Figure 5.7(b).

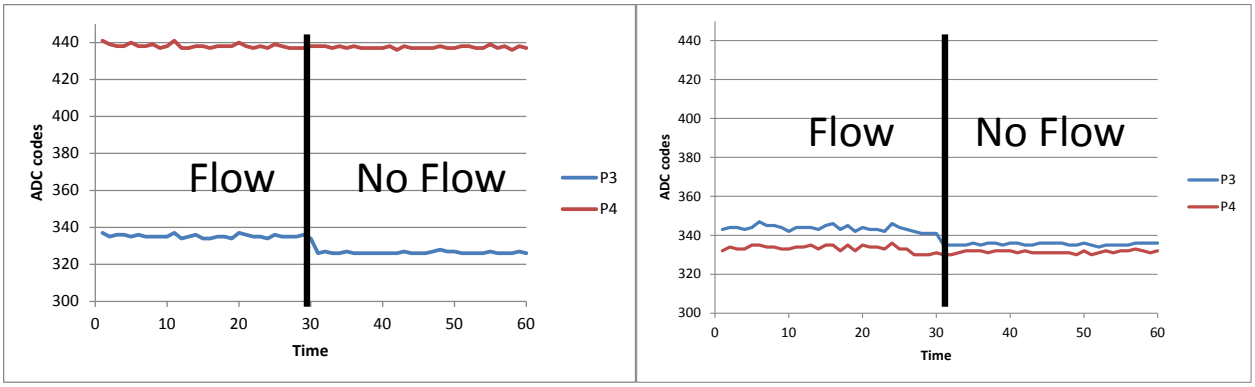

Figure 5.7. The pressure difference between two sensors at flow and no flow at (a) vertical position (b) horizontal position

Measuring the pressure in standing and supine position will help to calibrate the sensors online. If sensors S3 and S4 are at same height with respect to a reference in supine position, the pressure difference between the two sensors is due to the pressure drop due to flow.

The proposed calibration procedure and assumptions is as explained below

1) The sensor readings are measured at sitting and supine position after patient is recovered after surgery.
2) These readings are taken as the references. The vertical height differences of the sensors need to be noted at both the cases.
3) In horizontal position, if two sensors are in the same level and if the sensors are offset corrected, the pressure difference between them is the pressure drop due to flow. If the height difference between sensors is known, then decrease in static pressure proportional to flow.
4) This value of flow is calculated from flow calibration data.
5) If the flow rate is same for horizontal and vertical position, the pressure drop created between each sensor is the same as pressure drop is dependent only on the length of tube and velocity of flow.
6) Assuming accurate data for height difference between sensors are available at horizontal and vertical position, and the flow calibration data, sensor calibration can be done.

5.2.1 Posture-Pressure measurement and feedback control

The shunt valve is set at a particular setting for a patient. When the patient changes the posture from supine to sitting/standing as in Figure 5.8, there is additional hydrostatic pressure acting on the brain. This additional hydrostatic pressure increases the flow rate of CSF. When the posture of the patient changes from supine to standing, there is a decrease of ICP and an increase of IAP. This effectively reduces the increase of hydrostatic pressure. The ICP and IAP changes might be dependent on person to person and recording these two parameters will help to set the valve at an optimum position. Our sensors will be able to measure the increased hydrostatic pressure column. The difference of pressure between two sensors (S2-S1 & S4-S3) will capture this increased hydrostatic column. Thus system is able to determine the patient's posture.

To mimic the condition in Figure 5.8, the prototype system in Figure 4.3 is fixed to the surface of a wooden plank, where the position of one sensor w.r.t. each other remains the same. The plank is first placed in a horizontal position and the sensor readings and flow rate is measured. After the measurement is completed, the plank is tilted so that it is at angle w.r.t horizontal and the measurements are taken. The process is repeated until the plank is at a vertical position.

The posture measurement is done by finding the pressure difference between two sensors and the result are shown in Figure 5.9. The valve opening setting is held the same for all the postures. The sensors are mounted on a surface such that the position of each sensor with respect to others will not change during the measurement. The graph in Figure 5.9 shows the increased pressure difference measured between the sensors when the posture of the patient changed from

supine to standing. The flow rate increased due to the additional hydrostatic pressure in the shunt system due to gravity . For the external setting all the different postures are calibrated and the flow rate is calculated for all postures. When the system is implanted, calculating the flow rate at different postures will be difficult as obtaining a reference reading and calibrating it will be challenging. But these values can be estimated from the flow rate of CSF at standing and supine positions.

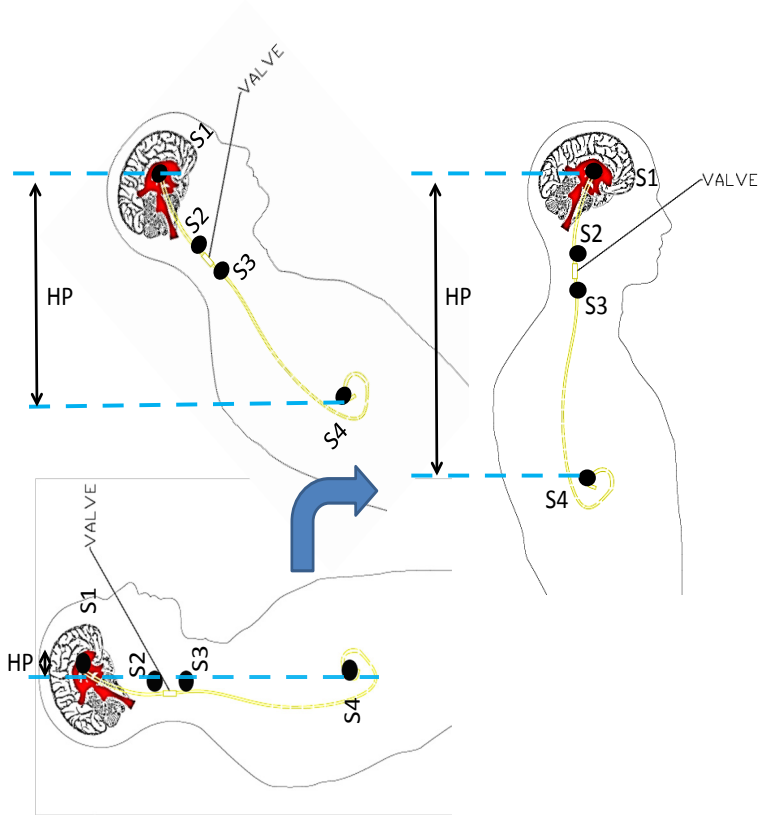

Figure 5.8. Sensor positions when patient is moving from a) supine posture to b) standing/sitting posture.

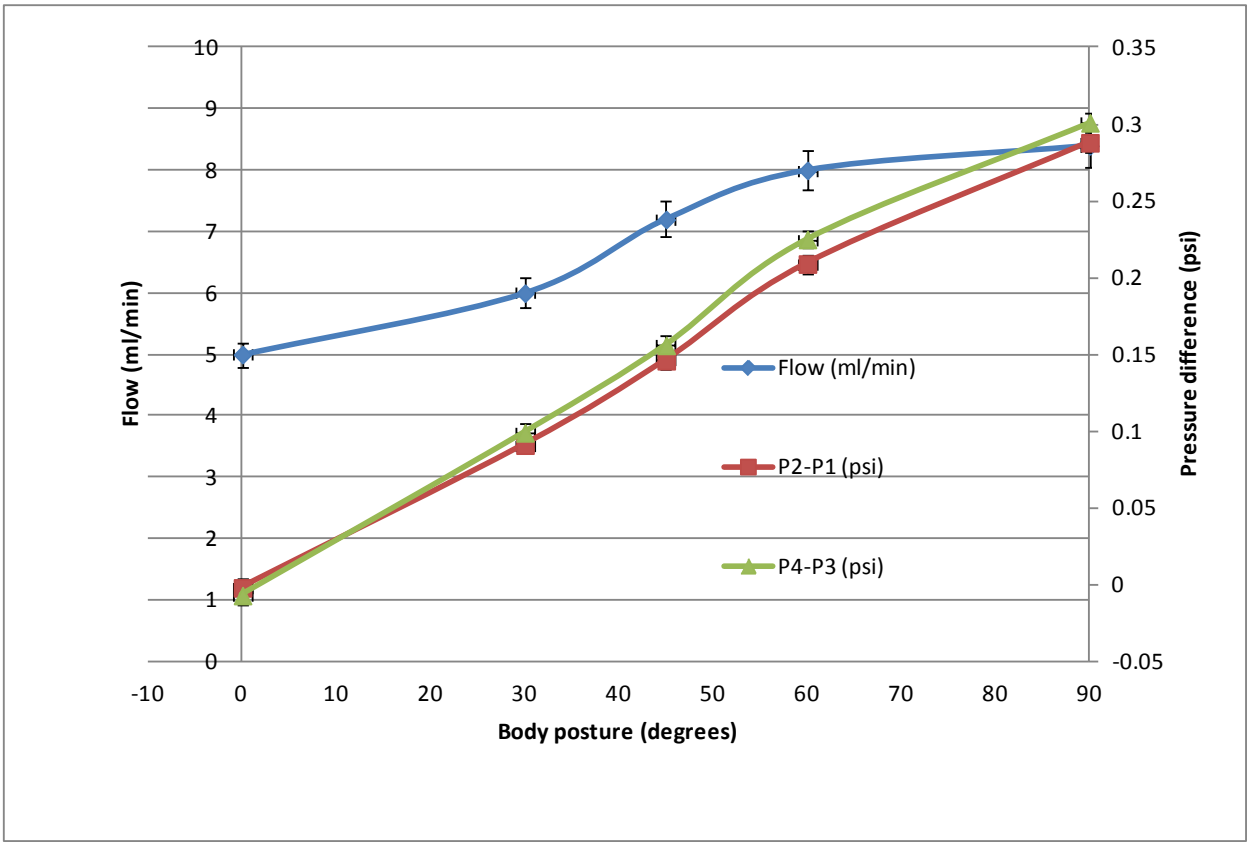

Figure 5.9. Flow rate (primary y-axis) and measured pressure difference (secondary y-axis) between pressure sensors at different body postures.

The prototype system is capable of detecting the posture of the patient and the corresponding flow rate. With continuous monitoring, the system can determine the posture of the patient and the respective flow rate. A feed-back control system can be designed with actuators to control the valve opening and closing position to optimize the flow rate. The system will take into account, the ICP, IAP. Valve opening and closing pressures, the posture of the patient in deciding the optimum flow rate. Continuous monitoring requires higher power and will need rechargeable batteries for providing uninterrupted power. Another approach is to monitor the flow rates, ICP

and IAP initially to get an understanding of the patient's normal range and set the valve accordingly for optimum flow rate. After that regularly monitor these values say once in an hour to monitor ICP. The valves can be adjusted based on periodical measurements if needed.

5.3 Online Calibration

For the application that involves implantable pressure sensors, the requirements include the device must be 1) small, 2)must be hermetic and biocompatible, 3) compatible with modern imaging techniques 4) have insignificant drift over time 5) comply with the required standards (FDA, ISO). The application determines the other design consideration like sampling rate, data transmission rate, sensitivity etc [1]. The pressure sensors used for our application is the MEMS based piezo-resitive sensors.

All the pressure sensors suffer from drift. The drift in catheter based sensor systems used for ICP measurements are usually handled by frequent recalibration (zeroing) through a reference pressure, usually atmospheric pressure. As the sensors are implanted, it is impossible to recalibrate without a surgery. The drifts in pressure sensors are basically of two kinds 1) offset drift and 2) sensitivity drift. Offset drift occurs when there is a change of sensor values from the calibrated state. For gage pressure sensors, usually the calibrated state is atmospheric pressure. During calibration, the offset voltage is found and it is corrected. The offset drift may be caused by aging of the sensing element or changes in reference pressure. Sensitivity drift causes a change in response to applied pressure corresponding to the initial response. The sensitivity drift may be caused by the mechanical fatigue of the sensor elements or even corrosion. The piezo-resistive pressure sensors, the materials used for sensor elements are temperature

dependent, which means both the offset drift and sensitivity drift are temperature dependent. Most of the commercially available sensors have innovative circuits to compensate for the effect of temperature.

5.3.1 Need of Calibration

Although the effect of drift due to temperature can be compensated, the offset drift and sensitivity drift due to aging needs to be compensated. As mentioned earlier, this is not possible to recalibrate the implanted sensors without a surgery; the options are to find a certain case in which pressure can be estimated so that sensors can be calibrated against that condition. By manufacturing very robust sensors, these offsets can be reduced, but it will be impossible to eliminate these offsets.

For our application, we are using multiple pressure sensors to determine the location of clog. We are using the pressure difference between sensors to calculate the flow through shunt. The pressure drop on the sensors is due to friction and is proportional to the length of the tube and velocity of flow. The pressure difference between any of the two sensors can be used to calculate flow at a given time and that must be the same. Flow rate at any particular point of time is calculated using all the possible sensor combinations and if the flow rate falls outside a certain margin of error in any one or more combinations, there is a probability of an offset drift.

The proposed procedure for online calibration is as follows.

1) The sensors in the shunt are calibrated for offset at atmospheric pressure.
2) After the shunt implant surgery, the sensor readings are measured in a standing and supine posture.

3) Using an imaging technique, the position of the sensors with respect to each other (It is also possible to measure the static pressure column by closing the valve and measuring the pressure sensor values).
4) From this data, calculate the static pressure difference measured between the sensors in standing and supine position
5) When there is a flow of CSF in the shunt, there is a reduction of pressure difference between the sensors. This pressure difference s due to frictional loss and is proportional to the length of the tube.
6) The pressure difference per unit length between any two sets of sensor is found and must be the same as the flow rate is the same throughout the shunt. This information is calculated from Step 2
7) The sources of error come from the ADC and noises and interferences. Depending on the system specification a suitable margin of error is calculated. (Mostly dependent on the resolution of ADC)
8) If the shunt is working fine, the sensor can be calibrated say once in 6 months or 1 year by repeating steps 2 and 6.
9) If the pressure difference per unit length changes below the margin, there is an offset change in sensor or sensors. If there is only offset change in one sensor, this change can be easily calculated.
10) If there is change in pressure in multiple sensors, more complex algorithm is needed for finding the offset

This proposed method will help to reduce high offset drift errors. Small errors within the tolerance margins are not corrected. Also small errors also can be induced due to small changes in postures during the initial measurements and the measurements for re-calibration. Also for the patients who are growing, there is also a need to redo steps 3 and 4 in the calibration as the respective position of the sensors is possible to change.

For the testing of the proposed calibration technique, the prototype was first offset corrected and the pressure differences between sensors are calculated at 3 chosen flow rates. From this a profile of the pressure difference per unit length to flow is obtained. To test the possible changes in the sensor offsets, one of the original sensors are replaced with another

sensor (5th sensor S5) with a different offset. The measurement conditions were made the same as before and the pressure data is found at the chosen flow rates. Each sensor is replaced by S5 one at a time and the pressure drop per unit length is calculated for the chosen flow rates.

5.3.2 Results

The four sensors S1, S2, S3 and S4 are offset corrected and pressure measured by each sensors are recorded using the prototype system for three different flow rates (15 ml/min, 20 ml/min, 24 ml/min). Then sensors S1 is replaced by S5 which has an offset different from the original four sensors, and pressure measured by the four sensors are recorded under the same conditions and at the chosen flow rates. Then other sensors (S2, S3, & S4) are also replaced by S5, and the pressure readings of the four sensors are recorded at the chosen flow rates. 100 data samples are collected for each of the flow condition and it is averaged out to obtain the pressure drop per unit length due to friction between the sensors. Ideally the frictional drop per unit length must be the same for any two sensor combination. Due to noise and ADC quantization, there is an error of up to ±1/2 LSB in the ADC reading. Tolerance level for the measurement is set at ±1 LSB and any standard deviation of the pressure drop between the sensors at a flow rate. Any SD less than that are cannot be used to calculate the offset drift.

In Figure 5.10, for case 1 where four offset corrected sensors are used, SD of pressure drop per unit area between each sensor is less than ½ LSB and that means there is no possible offset drift. When Sensor S1, S2, and S3 were replaced by S5, the SD increased and it increased appreciably. And in the case of S4, the SD is only above ½ LSB this is because the offset difference for S4 and S4 was only 1 LSB. Low offsets within an LSB of the ADC cannot be

reliably captured by this method. But very large offset drifts can be found out and corrected to increase the accuracy of flow. Also if more than one sensor offset drifts, with this method it is not possible to calculate offset drifts.

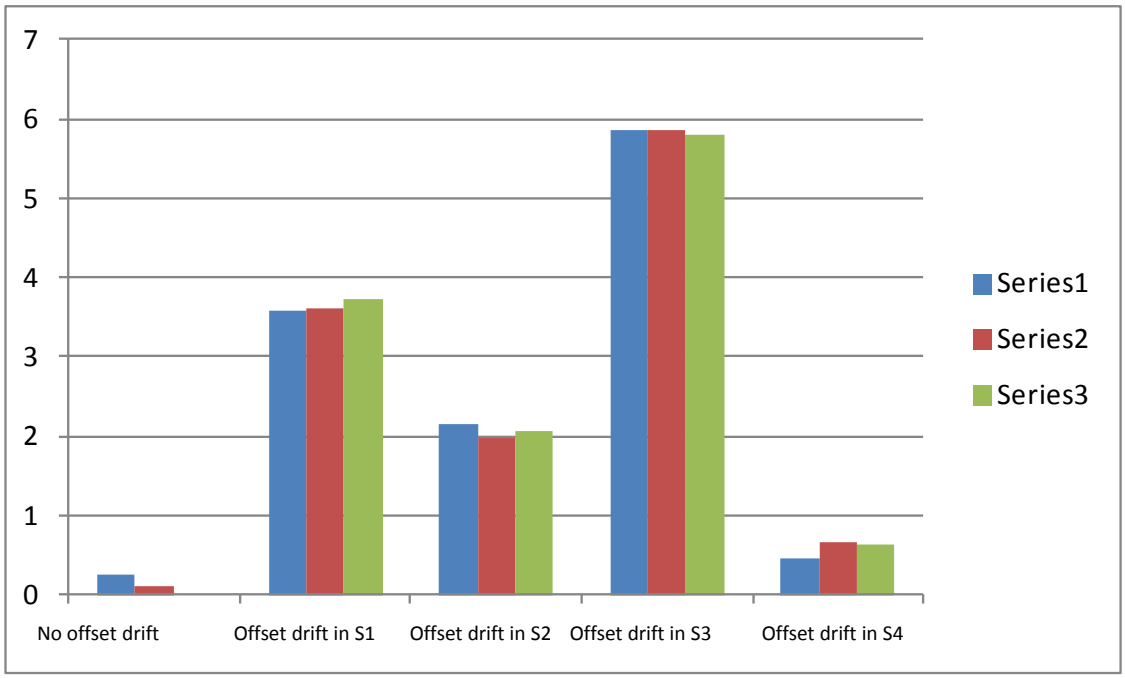

Figure 5.10. The SD of pressure drop/unit length at three chosen flow rates for offset corrected sensors and induced offsets in S1, S2, S3, and S4.

CHAPTER 6

CONCLUSION AND FUTURE DIRECTIONS

A lab prototype was designed for the detection of clog and flow measurement. The system uses multiple pressure sensors for finding the location of clog in the cerebrospinal fluid shunt. The system design involves the methodology for the detection of clog which is by comparing the pressure at different locations in the shunt. When there is a clog, there is a presence of a static column of CSF which gives rise to elevated pressure readings. The system detects the location of the clog with 100% accuracy needed for reducing the number of incisions needed for revision surgery when the measurement is taken in a sitting or standing position. The flow rate is also calculated using the pressure drop between the two sensors due to friction. The accuracy in flow rate is found to be 90%.

A transponder system was designed for the lab prototype which harvests power from an RF reader. The system design includes a custom designed PCB for the sensor interface circuit, power harvesting unit and data transmission unit. Power harvesting unit uses RF resonant powering and an 80 mA regulator which is able to provide a constant 3.3 V DC voltage to the components. The sensor interface uses minimum number of components and power consumed by this unit is only 0.47 mA of which 0.44 mA is used for sensor excitation. The sensor data is collected and transmitted to the reader. The designed GUI displays all the results including the clog location and flow rate. Also, there is an option of storing the data for further analysis.

The possibility of using the system beyond clog detection and flow measurement is explored. Using our system, it is possible to measure parameters such as ICP, IAP and pressure at various locations inside the shunt catheter. By monitoring these, medical staff can get a better understanding of parameters affecting the shunt as well as symptoms, progress and treatment of Hydrocephalus. With the additional information, there will be better shunt designs in future.

Future directions for this project may include the following

- The shunts are often implanted for long term, i.e. an average of 6 years to even the entire life of the patient. Aging of sensors and electronics after implant must be studied using accelerated testing. A systematic and periodic recalibration for sensors can be explored
- The proposed prototype only does on-demand sensor measurement. For continuous monitoring, a modified version of the system can be used. The present system could be incorporated with thin film rechargeable battery that can be charged quickly and efficiently using RF resonant powering and ability to store data in an internal memory.
- Miniaturization of the circuit and sensors so that an animal testing can be done. The present prototype is bulky and using off the-shelf sensors. The circuits must be made bio-compatible with suitable hermetic packaging.
- RF interference to communication circuitry must be explored. The literature offers generic platform to study interference but a comprehensive study needs special equipment such as spectrum analyzer and customized test set-up.

REFERENCES

[1] http://oreilly.com/medical/hydrocephalus/news/how_work.html

[2] http://www.ninds.nih.gov/disorders/hydrocephalus/hydrocephalus.htm

[3] M. Emam, Y. Abashiya, B. Chareunsack, J. Skordos, J.H. Oh, Y. Choi, F. Kralick, H. Noh. "A novel microdevice for the treatment of hydrocephalus: design and fabrication of an array of microvales and microneedles." *Microsyst. Technol* 2008.

[4] http://www.hydroassoc.org/

[5] www.medtronics.com

[6] A. Ahmed, G. Sandlas, P. Kothari, D. Sarda, A. Gupta, P. Karkera, P. Joshi. "Outcome analysis of shunt surgery in hydrocephalus." J Indian Assoc Pediatr Surg 2009.

[7] A.L. Albright, I.F. Pollack, P.D. Adelson, Principles and Practice of Pediatric Neurosurgery, New York: Thieme; 1999.

[8] R. V. Patwardhan, A. Nanda. "Implanted ventricular shunts in the United States: the billion-dollar-a-year cost of hydrocephalus treatment" *Neurosurgery 56:139-145, 2005.*

[9] http://www.medtronic.com/for-healthcare-professionals/products-therapies/neurological/shunts/index.htm

[10] http://www.depuysynthes.com/hcp/codman-neuro/products/qs/CODMAN-HAKIM-Programmable-Valve

[11] http://www.spiegelberg.de/products/shunt_systems.html

[12] S.R. Browd, B.T. Ragel "Failure of Cerebrospinal Fluid Shunts: Part I: Obstruction and Mechanical Failure," Pediatric Neurol, 34: 2, 2006.

[13] http://www.nphsurgery.org/Shunt-Malfunction-Theory-and-a-Proposed-Solution.html

[14] B.P. Wells. "Series resonant inductive charging circuit", US Patent 6 972 543, June 2005.

[15] P. Vaillancourt, A. Djemouai, J.F. Harvey, M. Sawan, "EM radiation behavior upon biological tissues in a radio-frequency power transfer link for a cortical visual implant," *Proceedings of the 19th Annual International Conference of the IEEE*, vol. 6, pp. 2499-2502, Nov. 1997.

[16] K. Finkenzeller, RFID Handbook: Fundamentals and Applications in Contactless Smart Cards and Identification, 2nd ed. New York, John Wiley & Sons, Inc., 2003.

[17] M.R. Haider, S.K.Islam, S. Mostafa, M. Zhang, O. Taeho, "Low-Power Low-Voltage Current Readout Circuit for Inductively Powered Implant System,"*Biomedical Circuits and Systems, IEEE Transactions on* , vol.4, no.4, pp.205,213, Aug. 2010

[18] A. Ginggen, Y. Tardy, R. Crivelli, T. Bork, P. Renaud, "A Telemetric Pressure Sensor System for Biomedical Applications," *Biomedical Engineering, IEEE Transactions on* , vol.55, no.4, pp.1374,1381, April 2008

[19] C. Hierold, B. Clasbrumme, D. Behrend, T. Scheiter, M. Steger, K. Oppermann, H. Kapels, E. Landgraf, D. Wenzel, D. Etuodt, "Implantable low power integrated pressure sensor system for minimal invasive telemetric patient monitoring," *MEMS 98. Proceedings., The Eleventh Annual International Workshop on* , vol., no., pp.568,573, 25-29 Jan 1998

[20] M. A. Adeeb, A. B. Islam, M. R. Haider, F. S. Tulip, M. N. Ericson, and S. K. Islam, "An Inductive Link-Based Wireless Power Transfer System for Biomedical Applications," Active and Passive Electronic Components, vol. 2012, Article ID 879294, 11 pages, 2012. doi:10.1155/2012/879294

[21] R. Puers, K. V. Schuylenbergh, M. Catrysse and B. Hermans, "Wireless inductive transfer of power and data," Analog Circuit Design, Springer, (2006)

[22] M. Sole, A. Sanni, A. Vilches, C. Toumazou, T.G. Constandinou. "A bio-implantable platform for inductive data and power transfer with integrated battery charging," Circuits and Systems (ISCAS), 2011 IEEE International Symposium on, vol., no., pp.2605,2608, 15-18 May 2011

[23] S. Majerus "Wireless, ultra-low-power implantable sensor for chronic bladder pressure monitoring," ACM Journal of Emerging Technology, vol. 8, no. 2, pp. 11.1-11.13, 2012.

[24] C. Li, P.M.Wu, J. Han, C.H. Ahn, "A flexible polymer tube lab-chip integrated with microsensors for smart microcatheter," Biomed. Microdevices pp. 671-679, 2008.

[25] R.E. Oosterbroek, T.S.J. Lammerink, J.W. Berenschot, G.J.M. Krijnen, M.C. Elwenspoek, and A. vanden Berg, "A micromachined pressure/flow-sensor," Sensors and Actuators **77**, 167 (1999).

[26] N.T. Nguyen, "Micromachined flow sensors-a review," Flow Meas. Instrum. **8**, 7 (1997).

[27] M Czosnyka, J Pickard. Monitoring and interpretation of intracranial pressure. J Neurol Neurosurg Psychiatry, 75 (2004), pp. 813–821

[28] Shi W, Saito I, Chinzei T, Isoyama T, Miura H, Kouno A, Ono T, Nakagawa H, Yamaguchi S, Inoue Y, Kishi A, Abe Y. "Development of an auto-calibration method for the implantable blood pressure sensor in the undulation pump ventricular assist device (UPVAD)." IFMBE Proceedings. 2008; 19:66-69

[29] http://www.neuros.net/en/about_hydrocephalus.php

[30] Malm, Jan, et al. "Cerebrospinal fluid shunt dynamics in patients with idiopathic adult hydrocephalus syndrome." *Journal of Neurology, Neurosurgery & Psychiatry* 58.6 (1995): 715-723.

[31] http://www.sensirion.com/en/products/liquid-flow-sensors/

[32] C.A Harris, J.P. McAllister . "Does drainage hole size influence adhesion on ventricular catheters?" Childs Nerv Syst 2011;27:1221-32.

[33] W.H. Ko, C.W. Meyrick, H.L. Rekate. Cerebrospinal-Fluid Control-System. Proc. IEEE1988; 76:1226-35.

[34] W. Bertrand, D. Harper, L.Speckman, A. Kiehl, R. Scheer . Implantable cerebral spinal fluid drainage system. U.S. Patent 7309330, issued Dec. 18, 2007.

[35] K. Miesel, L. Stylos . Intracranial monitoring and therapy delivery control device, system, and method. U.S. Patent 6248080, issued Jun. 19, 2001

[36] L. Ludin , C. Mauge . Programmable shunt with electromechanical valve actuator. U.S. Patent US8123714, issued Feb. 28, 2012.

[37] http://ccmctraining.com/peds_html_fixed/images/ei_0433.gif

[38] http://archive.wired.com/testguide/fall2006/images/household/1306WIHSHOUS024.jpg

[39] http://www.designnews.com/photo/285/285087-Cymbet_Corp_s_EVAL_11_EnerChip_RF_Induction_Charging_Kit_A.jpg

[40] http://www.rfwirelesssensors.com/img/rf-energy-harvesting-credit-card.jpg

[41] G. Jiang. "Design challenges of implantable pressure monitoring system." Front. Neurosci. 4:29. doi: 10.3389/neuro.20.002.2010

[42] I.G. Bloomfield, I.H Johnston, L.E Bilston. Effects of proteins, blood cells and glucose on the viscosity of cerebrospinal fluid. Pediatr Neurosurg 28: pp. 246 –251, 1998.

[43] E. Levin, S. Muravchick, M.I. Gold. Density of human cerebrospinal fluid and tetracaine solutions. Anesth Analg: pp. 814-817, 1981.

[44] J. Sotelo. " The hydrokinetic parameters of shunts for hydrocephalus might be inadequate. Surg Neurol Int, 2012

[45] J Malm, B. Kristensen, T. Karlsson, M. Fagerlund, J. Elfverson, J. Ekstedt "The Predictive Value of Cerebrospinal Fluid Dynamic Tests in Patients With the Idiopathic Adult Hydrocephalus Syndrome." *Arch Neurol.* pp. 783-789, 1995.

[46] A.R. Alkharabsheh, L. Momani, N. Al-Zubi, W. Al-Nuaimy. "A Multi-Agent Approach for Self-Diagnosis of a Hydrocephalus Shunting System." In: Developments in E-systems Engineering (DESE), 2010.

[47] A.R. Alkharabsheh, L. Momani, N. Al-Zubi, W. Al-Nuaimy. "An expert system for hydrocephalus patient feedback." Conf Proc IEEE Eng Med Biol Soc 2010; 2010.

[48] N. Al-Zubi, A.R. Alkharabsheh, L. Momani, W. Al-Nuaimy. "Intelligent shunt agent for gradual shunt removal." Conf Proc IEEE Eng Med Biol Soc 2010; 2010.

[49] S. Jetzki, M.Kiefer, R.Eymann, M. Walter, S.Leonhardt." Analysis of Pulse Waves in Intracranial Pressure." Conf Proc IEEE Eng Med Biol Soc 2007; 2007.

[50] S. Jetzki, M. Kiefer, M. Walter, S. Leonhardt . "Concepts for a mechatronic device to control intracranial pressure." In 4th IFAC Symposium on Mechatronic Systems. Heidelberg, Germany: 2006.

[51] S. Jetzki, S. Leonhardt. "An electronic implant for Hydrocephalus therapy assistance." Conf Proc IEEE Eng Med Biol Soc 2008; 2008.

[52] I.M. Elixmann, M. Walter, C. Goffin, S. Hahne, M. Kiefer, S. Leonhardt. "Brain Pressure Modelling and Automatic Control of a New Mechatronic External Ventricular Drainage." At-Automatisierungstechnik 2011.

[53] G.L Cote, R. Durai, B. Zoghi. "Nonlinear Closed-Loop Control-System for Intracranial-Pressure Regulation." Ann Biomed Eng 1995.

[54] H. J. Yoon, J. M. Jung, J. S. Jeong, S. S. Yang. "Micro devices for a cerebrospinal fluid (CSF) shunt system." Sens Actuator A-Phys 2004.

[55] G. Thomas, R. Farrow, S. Liu. "No clog shunt using a compact fluid drag path." U.S. Patent 8088091, issued Jan. 3, 2012.

[56] S. Szczesny, S. Jetzki, S. Leonhardt. "Review of Current Actuator Suitability for Use in Medical Implants." Conf Proc IEEE Eng Med Biol Soc 2006.

[57] S. Bottan, D. Poulikakos, V. Kurtcuoglu. "Phantom Model of Physiologic Intracranial Pressure and Cerebrospinal Fluid Dynamics." IEEE Trans Biomed Eng 2012.

[58] S. Basati, B. Desai, A. Alaraj, F. Charbel, A. Linninger. "Cerebrospinal fluid volume measurements in hydrocephalic rats." J Neurosurg Pediatr 2012.

[59] S. Basati, T. J. Harris, A. Linninger. "Dynamic brain phantom for intracranial volume measurements." IEEE Trans Biomed Eng 2011.

[60] A. Linninger, S. Basati, R. Dawe, R. Penn. "An impedance sensor to monitor and control cerebral ventricular volume." Med Eng Phys 2009;31:838-45.

[61] A. Linninger. "Monitoring and controlling hydrocephalus," In: WIPO, editor. US Patent App. 20100130884, filed Jul. 2, 2007.

[62] http://www.ghadialisurgery.com/pdf/hydrocephalus.pdf

VITA

Anand Narayanaswamy was born in Kottayam, Kerala, India. After completing his schoolwork at Marian Junior School in Kottayam, Anand started his Bachelor of Technology degree in Electrical Engineering at Mahatma Gandhi University, Kottayam. He received his BS in Electrical Engineering with first class in July 2006. He then joined for his Master of Science Degree in Electrical Engineering at Case Western Reserve University, Cleveland, Ohio. There he completed his MS with thesis "A Non-contact Sensor Interface for High Temperature, MEMS Capacitive Sensors" in August 2010. He started PhD at UT Dallas in August 2010.